



## Original Articles

## Biphasic co-detection of melanoma aneuploid tumor cells and tumor endothelial cells in guidance of specifying the field cancerized surgical excision margin and administering immunotherapy

Zhengzheng Fu<sup>a,1</sup>, Lina Zhang<sup>b,1</sup>, Rongyi Chen<sup>c</sup>, Jipang Zhan<sup>a</sup>, Jing Zhong<sup>a</sup>, Wen Zheng<sup>a</sup>, Jingwen Zou<sup>a</sup>, Peng Wang<sup>d</sup>, Xiaohua Deng<sup>d</sup>, Alexander Y. Lin<sup>e</sup>, Daisy Dandan Wang<sup>e</sup>, Peter Ping Lin<sup>e,\*\*</sup>, Renliang He<sup>a,\*</sup>

<sup>a</sup> Department of Dermatologic Surgery and Dermatologic Oncology, Dermatology Hospital of Southern Medical University, Guangdong Provincial Dermatology Hospital, Guangzhou, China

<sup>b</sup> Department of Cellular and Molecular Biology, Beijing Chest Hospital, Capital Medical University, Beijing Tuberculosis and Thoracic Tumor Research Institute, Beijing, China

<sup>c</sup> Division of Cutaneous Oncology, Department of Dermatology, Dermatology Hospital of Southern Medical University, Guangdong Provincial Dermatology Hospital, Guangzhou, China

<sup>d</sup> Department of Pathology, Dermatology Hospital of Southern Medical University, Guangdong Provincial Dermatology Hospital, Guangzhou, China

<sup>e</sup> Cytelligen, San Diego, CA, USA

## ARTICLE INFO

## Keywords:

Quantified field cancerization  
Safety excision margin  
Cellular MRD  
Aneuploid CTCs and CTECs  
iFISH tumor tissue and liquid biopsies

## ABSTRACT

An optimum safety excision margin (EM) delineated by precise demarcation of field cancerization along with reliable biomarkers that enable predicting and timely evaluating patients' response to immunotherapy significantly impact effective management of melanoma. In this study, optimized biphasic "immunofluorescence staining integrated with fluorescence *in situ* hybridization" (iFISH) was conducted along the diagnosis-metastasis-treatment-cellular MRD axis to longitudinally co-detect a full spectrum of intact CD31<sup>-</sup> aneuploid tumor cells (TCs), CD31<sup>+</sup> aneuploid tumor endothelial cells (TECs), viable and necrotic circulating TCs (CTCs) and circulating TECs (CTECs) expressing PD-L1, Ki67, p16 and Vimentin in unsliced specimens of the resected primary tumor, EM, dissected sentinel lymph nodes (SLNs) and peripheral blood in an early-stage melanoma patient. Numerous PD-L1<sup>+</sup> aneuploid TCs and TECs were detected at the conventional safety EM (2 cm), quantitatively indicating the existence of a field cancerized EM for the first time. Contrary to highly heterogeneous PD-L1 expression and degrees of Chr8 aneuploidy in TCs and TECs in the primary lesions as well as CTCs and CTECs in peripheral blood, almost all TCs and TECs in SLNs and EM were homogeneously PD-L1<sup>+</sup> haploid cells. Dynamic monitoring and cellular MRD assessment revealed that, in contrast to PD-L1<sup>+</sup> CTCs being responsive to the immune checkpoint inhibitor (ICI-anti-PD-1), multiploid ( $\geq$ pentasomy 8) PD-L1<sup>+</sup> and Ki67<sup>+</sup> CTECs were respectively resistant to ICI-sensitized T cells. In therapeutically stressed lymphatic and hematogenous metastatic cascades, stratified phenotypic and karyotypic profiling of iFISH tissue and liquid biopsied TCs, TECs, CTCs and CTECs in future large-cohort studies will enable appropriate re-specification of the optimal safety EM and distribution mapping of in-depth characterized, subcategorized target cells to help illustrate their metastatic relevance, ultimately improving risk stratification and clinical intervention of tumor progression, metastases, therapy resistance and cancer relapse.

\* Corresponding author.

\*\* Corresponding author.

E-mail addresses: [plin@cytelligen.com](mailto:plin@cytelligen.com) (P.P. Lin), [zshrl2006@smu.edu.cn](mailto:zshrl2006@smu.edu.cn) (R. He).

<sup>1</sup> ZF and LZ are co-first authors.

<https://doi.org/10.1016/j.canlet.2024.217099>

Received 14 April 2024; Received in revised form 18 June 2024; Accepted 29 June 2024

Available online 4 July 2024

0304-3835/© 2024 The Authors. Published by Elsevier B.V. This is an open access article under the CC BY license (<http://creativecommons.org/licenses/by/4.0/>).

## 1. Introduction

Melanoma, derived from epithelial cell adhesion molecule (EpcAM)-negative melanocytes, is a rare but the most invasive cutaneous cancer with the highest risk of mortality. With steadily increasing incidents, melanoma accounts for 75 % of skin cancer mortality although accounting for only 4 % of skin cancer morbidity (American Cancer Society). A great endeavor of treatment efforts, including mono- or combined regimens of surgical resection, adjuvant or neoadjuvant immunotherapy, targeted therapy, photodynamic therapy, chemo- or biochemotherapy and nano-drug delivery targeting the melanoma tumor microenvironment have significantly improved clinical management of melanoma [1–6].

Complete lymph node dissection (CLND) to remove sentinel lymph node biopsy (SLNB)-positive lymph nodes (LNs) demonstrates time-dependent benefits to melanoma patients [7,8], but all rely on a timely and correct pathological biopsy. Surgical resection is the primary choice of management for melanoma patients staging I-IIIb [2]. Histopathology biopsy defined excision margin of up to 2 cm from the tumor edge is currently recognized as the standard safety excision margin for melanoma resection [2,9]. Following recognition of the concept “field cancerization” (FC) [10–12], its outstretched region beyond the primary foci, which consist of histopathologically unrecognizable field cancerized cells exhibiting normal cell morphology [11,12], challenges the conventional safety excision margin with respect to postoperative cellular minimal residual disease (MRD)-derived recurrence.

Aside from eligible excision, immune checkpoint inhibition (ICI) administered as the primary immunotherapy has revolutionized systemic treatment paradigm for malignant melanoma and shown sustained remission [2,13–15]. Post-surgical adjuvant ICI immunotherapy has demonstrated both recurrence-free survival and overall survival benefit [16]. The immunotherapeutic efficacy is, however, affected by the immunogenic tumor microenvironment (TME). TME, fostered for cancer development and metastasis, is mainly constituted of tumor blood vessels, infiltrating inflammatory cells, stroma cells and proliferating neoplastic cells with cytogenetic abnormalities of aneuploidy. Melanoma cells in the TME are highly regulated by several signaling pathways including the MGRN1-dependent pathway [17]. Aneuploidy, the hallmark of carcinoma cells [18,19], dynamically potentiates chromosomal instability that leads to further karyotype diversity in aberrant host cells [20,21]. The degree of diverse karyotypic aneuploidy is proportional to the grade of malignancy [22]. Chromosomal aneuploidy affects multiple genes' transcription in cancer cells, resulting in a profound variety of phenotypes that contribute toward tumor heterogeneity and therapeutic drug resistance in either patients with different types of cancers including melanoma [23–25] or metastatic patient-derived xenograft (mPDX) tumor animal models [26]. In the TME, the tumor suppressor gene *CDKN2A* encoded p16INK4a (p16), one of the major cell cycle checkpoints that inhibits CDK 4/6 complex binding to cyclin D1, functions as a robust cell cycle regulator and tumor suppressor protein. Attenuated expression or loss of p16 correlates with highly increased cell proliferation indexed by Ki67, resulting in enhanced metastasis and poorer clinical outcomes in patients with the most aggressive melanoma [27]. Moreover, positive expression of mesenchymal marker protein in melanoma cells, such as intracellular Vimentin, was reported to associate with patients' inferior prognosis [28].

Unlike conventional endothelial cells (ECs) in normal blood vessels, ECs in tumor vasculature in the TME are termed as tumor endothelial cells (TECs), exhibiting aneuploid chromosomes and positive expression of CD31 [29]. Aneuploid CD31<sup>+</sup> TECs are predominately derived from endothelialization of tumor cells (TCs) and cancerization of endothelial cells through processes of TCs-ECs fusion and/or transdifferentiation of TCs to TECs in the hypoxic TME [30], thus bearing dual properties of both ECs and malignant tumor cells. Contributions of TECs to tumor angiogenesis and progression as well as inhibition of immune functions

have been recently highlighted [31]. Similar to circulating tumor cells (CTCs), aneuploid TECs turn into CD31<sup>+</sup> aneuploid circulating TECs (CTECs) following their shedding from the lining of the neoplastic vasculature wall into peripheral blood [30,32]. Of particular interest are CTECs that substantially express a variety of tumor and cancer immunotherapy-related stemness markers [33–35]. Clinical utilities of CTECs [36,37] and its clusters [38] in multiple types of cancer patients have been investigated. CTECs were found to correlate with neoadjuvant chemotherapeutic efficacy in breast cancer patients [39]. In addition, PD-L1<sup>+</sup> CTECs were resistant to the ICI agent nivolumab-based immunotherapy and correlated with poor outcomes in non-small cell lung cancer (NSCLC) patients [36].

Apart from ICI's benefits to patients, a substantial subset of melanoma, however, possesses inherent or develops *de novo* or acquired resistance to immunotherapy, which significantly undermines its clinical implementation [40,41]. Thus, there is an imperative yet unmet need for a comprehensive strategy integrating tumor tissue biopsy and tumor liquid biopsy capable of co-detection and in-depth characterization of TCs, TECs, CTCs and CTECs in primary tumor lesions and peripheral circulation. This will improve risk assessment and stratification, identification of subjects eligible for treatment, effective evaluation of treatment efficacy in real time and timely monitoring of emerging resistance during therapy. Several intriguing questions, including whether and how the existing safety excision margin which is closely tied with histopathologically unrecognizable field cancerization has an impact on patients' post-surgical relapse and how quantitative *in situ* phenotypic and karyotypic molecular biopsy assists conventional histopathology biopsy to provide more precise molecular diagnosis of metastasis in LNs and distant organs, are yet to be investigated.

In the present study, optimized iFISH tumor tissue biopsy and EpcAM-independent SE-iFISH tumor liquid biopsy (subtraction enrichment integrated with immunofluorescence staining-fluorescence *in situ* hybridization) [32,37,42] were utilized to longitudinally co-detect and comprehensively characterize a full spectrum of melanoma aneuploid TCs and TECs at multiple locations including primary tumor, excision margin, sentinel lymph nodes (SLNs) and peripheral blood throughout therapy. Cellular tri-element (aneuploidy, tumor marker expression and cell morphology)-based iFISH [32,43] detected and characterized several subcategories of melanoma aneuploid TCs, TECs, viable and necrotic CTCs and CTECs [44] expressing programmed death-ligand 1 (PD-L1 or CD274, the ligand for the immune checkpoint programmed cell-death 1 protein known as PD-1), Ki67, p16 and/or Vimentin. Obtained results were consistent with previous studies showing that comprehensive characterization of co-detected CTC and CTEC subpopulations rather than enumeration of cell number alone could significantly expand clinical utilities of CTC [45]. Moreover, the relevance of those cells located at different sites in lymphatic and hematogenous metastatic cascades was further examined. Beyond detecting PD-L1<sup>+</sup> melanoma TCs and TECs to assist administration of post-surgical adjuvant ICI immunotherapy, additional achievements of combined tumor tissue and liquid molecular biopsies, including probing the field cancerized excision margin, comprehensively diagnosing metastatic SLNs, longitudinally evaluating therapeutic efficacy in real time and timely detecting cellular MRD of CTCs and CTECs, help pave the way for future large-cohort comprehensive clinical studies, ultimately facilitating more effective intervention of cancer metastases and improvement in clinical management of patients with melanoma and other types of cancers.

## 2. Materials and methods

### 2.1. Description of the patient

A 57-year-old healthy female Hong Kong resident, who had no family history of genetic disease or cancer, worked in a manufacturing factory with no exposure to toxic or radioactive materials. The subject presented

with a non-diabrosin dark patch on her right pelma skin for five years. The skin patch became darker in color, accompanied by exudate, hemorrhage per diabrosin, obscure boundary and inhomogeneous pigments in the past four months. The subject was admitted to the Southern Medical University Affiliated Dermatology Hospital and diagnosed with a non-invasion primary cutaneous malignant melanoma in a size of 2.5 × 1.5 cm (T3aN0M0, stage IIA, AJCC 8th edition) on June 30, 2023. The patient had several enlarged lymph nodes (LNs) with hypermetabolic activities located at bilateral groins and bilateral iliac blood vessels revealed by PET/CT scan. Those enlarged LNs were diagnosed with benign inflammatory hyperplasia. Aneuploid CTCs and CTECs including Vimentin (Vim)<sup>+</sup> CTCs in patient's blood were concurrently identified by SE-iFISH when the subject was diagnosed with melanoma.

The patient was subjected to surgical resection on July 11, 2023, with a conventional safety excision margin of 2 cm from the tumor edge [2,9]. iFISH tumor tissue biopsy performed on both resected primary tumor and excision margin site detected the presence of aneuploid TCs and TECs with a high expression of PD-L1 and additional tumor markers. In conjunction, SE-iFISH liquid biopsy was carried out and detected PD-L1<sup>+</sup> aneuploid CTCs and CTECs in patient's peripheral blood a week post-surgery. Accordingly, the subject received adjuvant ICI monotherapy. Anti-PD-1 Toripalimab (Junshi Biosciences, Shanghai, China) was intravenously administered at 186 mg/cycle for total of 12 cycles. Longitudinal SE-iFISH liquid biopsy was applied to timely monitor therapeutic efficacy. Because viable aneuploid CTCs and CTECs were consistently detected following two cycles of immunotherapy, nodal clearance by CLND, as a preventative procedure, was carried out to dissect entire enlarged sentinel LNs (SLNs). Subsequent iFISH tissue biopsy confirmed a positive result to SLNB, showing the existence of PD-L1<sup>+</sup> TCs and TECs in two of three biopsied SLNs. The patient received the last cycle of ICI treatment on December 29, 2023, followed by SE-iFISH detection of MRD CTCs and CTECs on January 15, 2024. Dramatically increased ICI-resistant MRD CTCs and CTECs were detected. The patient is currently receiving traditional Chinese herb medicine treatment according to her willingness.

The informed consent form, approved by the Ethics Review Committees (ERC) of the Dermatology Hospital, Southern Medical University, was signed and obtained from the patient prior to sample collection. The clinical study was performed according to the Declaration of Helsinki Principles.

## 2.2. Biphasic iFISH tumor tissue and liquid biopsies

### 2.2.1. iFISH tumor tissue biopsy

Excised melanoma and excision margin specimens, as well as dissected lymph nodes were respectively stored in the Tissue Preservation Solution (Cytelligen, San Diego, CA, USA) and subsequently subjected to homogenization to prepare intact individual cells in suspension, followed by iFISH processing described below.

### 2.2.2. SE-iFISH tumor liquid biopsy

Subtraction Enrichment (SE)-iFISH (Cytelligen) was performed as previously published with minor modifications [32,37,46]. CTCs and CTECs in blood were enriched by subtraction enrichment (SE), followed by iFISH analysis. Briefly, 3 ml of blood containing ACD anti-coagulant were spun down at 200×g for 15 min at room temperature to deplete supernatant plasma. Sedimented blood cells resuspended with 3 ml hCTC buffer were loaded on the non-hematologic cell separation matrix. Samples were centrifuged at 450×g for 5 min, followed by collecting the WBC-containing solution above RBC layer. Solution was incubated with magnetic beads conjugated to a cocktail of anti-WBC mAbs. WBCs-bound immuno-beads were subsequently depleted using a magnetic grate. The remaining non-hematologic cells were mixed with the cell fixative, then smeared on the formatted CTC slides and dried for subsequent iFISH processing.

Six-color iFISH was performed according to the manufacturer's

protocol (Cytelligen). Briefly, dried monolayer cells on coated slides were dehydrated and subjected to FISH hybridization with the chromosome 8 centromere probe (CEP8 Spectrum Orange, Vysis, Abbott Laboratories, Chicago, IL, USA, approved by USFDA for identification of solid tumor cells) for 3 h utilizing a ThermoBrite FISH Slides Processing System (Leica Biosystems, Buffalo Grove, IL, USA). Samples were subsequently incubated with indicated fluorescent monoclonal antibodies, respectively including Alexa Fluor (AF488) or Cyanine 5 (Cy5) conjugated anti-PD-L1 (Clone 29E.2A3, Dana-Farber Cancer Institute, Harvard Medical School, Boston, MA, USA), Cy5 or Cy7-anti-CD31 (Clone WM59), AF594 or Cy5-anti-CD45 (Clone 9.4), AF488-anti-Ki67 (Clone 19), AF594-anti-p16 (C-terminal), Cy7-anti-Vimentin (Clone 1D3) and the necrotic cell staining (NCS) reagent [44]. Following washing, the iFISH Full Spectrum Anti-Fade Mounting Medium with DAPI (Cytelligen) was added to specimens, then slides were subjected to automated image scanning and analysis described below. All antibody conjugation was performed in house at Cytelligen.

### 2.2.3. Automated CTC 3D scanning and image analysis

The formatted CTC slides were automatically scanned and analyzed utilizing the Metafer-i•FISH imaging system co-developed by Carl Zeiss (Oberkochen, Germany), MetaSystems (Altlussheim, Germany) and Cytelligen. Cells on the slide were subjected to 3D scanning with cross Z-sectioning at 1 μm-steps of depth in each fluorescence channel, including AF488 (green), AF594 (red), Cy5 (yellow), Cy7 (pink), CEP8 (orange) and DAPI (blue). Identification criteria for aneuploid CD31<sup>-</sup> TCs and CTCs included: DAPI<sup>+</sup>/CD45<sup>-</sup>/CD31<sup>-</sup>/tumor marker<sup>+</sup> or<sup>-</sup>/CEP8≠2 (except tumor marker<sup>+</sup> near-diploid)/cells; criteria for aneuploid CD31<sup>+</sup> TECs and CTECs included: DAPI<sup>+</sup>/CD45<sup>-</sup>/CD31<sup>+</sup>/tumor markers<sup>+</sup> or<sup>-</sup>/CEP8≠2 (except tumor marker<sup>+</sup> near-diploid)/cells. Small cell: ≤5 μm; large cell: >5 μm. Comprehensive characterization and subcategorization of aneuploid CTCs and CTECs were performed upon cell size, cell cluster, tumor marker expression and the degree of aneuploidy.

## 3. Results

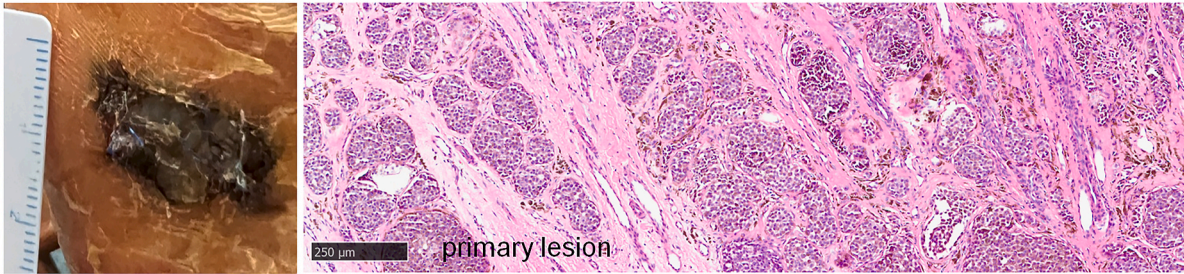
### 3.1. Pathological diagnosis of melanoma and enlarged sentinel lymph nodes

Representative images of cutaneous melanoma, which was pathologically biopsied by routine H&E and immunohistochemistry (IHC) staining (Dept. of Pathology, Dermatology Hospital of Southern Medical University), are demonstrated in Fig. 1A and B. No lymphatic or blood vessel invasion and no tumor infiltrating lymphocytes were observed in the biopsied melanoma specimen.

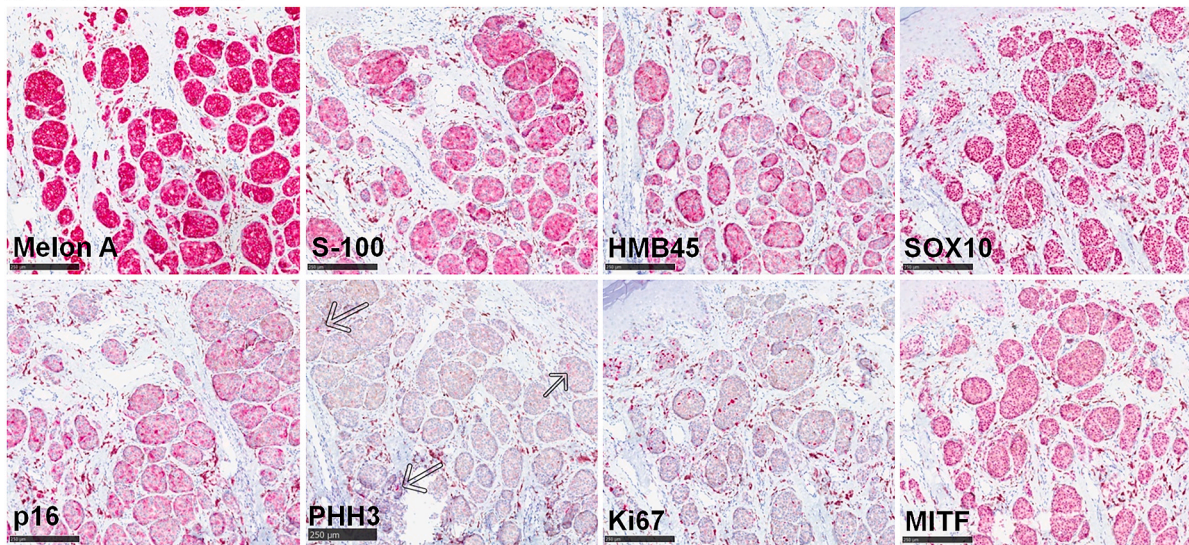
Pathological diagnosis of melanoma at patient's right planta was further confirmed by whole-body PET/CT scan, showing irregular focal hypermetabolic activities at the same lesion area (Fig. 1C). Several enlarged SLNs located at bilateral groins and bilateral iliac blood vessels were revealed by PET/CT scan (Fig. 1C), with some displaying hypermetabolic activities as indicated by red arrows. Enlarged SLNs were diagnosed with benign inflammatory hyperplasia by medical imaging modalities of subcutaneous color Doppler ultrasonography and PET/CT. The primary melanoma foci was surgically excised. In view of consistent positive detection of CTCs and CTECs following initiation of post-operative adjuvant immunotherapy, preventative nodal clearance of enlarged SLNs was performed 72 days post-surgery or 55 days since therapy initiation. Histopathology biopsy of dissected SLNs suggested that possible melanoma metastasis could not be ruled out (Fig. 1C). Concurrent iFISH tissue biopsy showed positive SLNB, confirming the existence of TCs and TECs in two of three biopsied SLNs.

Melanoma-related 13-gene mutation analysis indicated the existence of an activating mutation in the *NRAS* oncogene, designated as NM\_002524:c.181C > A (p. Q61K), with a mutation frequency of 44.1 % (Fig. 1D) (KingMed Diagnostics, Guangzhou, China). NRAs<sup>Q61K</sup>

**A H&E staining**



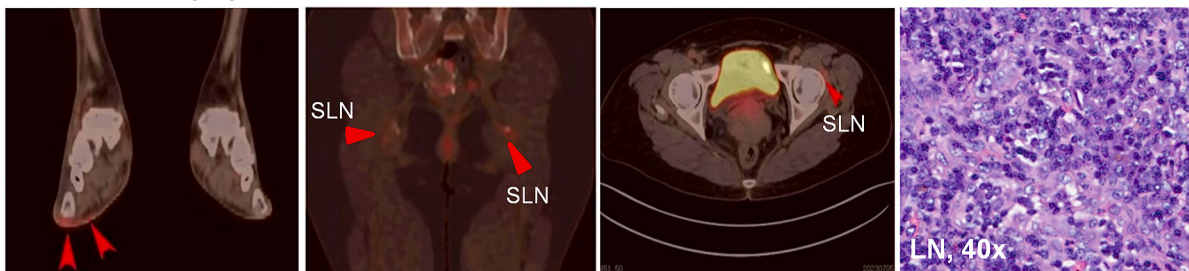
**B IHC examination**



**Summary of IHC**

Markers	Melan A	S-100	HMB45	SOX10	p16	PHH3	Ki67	CD34	D2-40	MITF
Results	+	+	+	+	+	3/HPF	5%	-	-	+

**C Medical imaging**



**D Melanoma-relevant gene mutation examination**

Genes	NRAS	BRAF	PTEN	GNAQ	BRCA2	GNA11	CDKN2A	CTNNB1	MAP2K1	CDK4	TP53	KIT	NF1
Mutations	Q61K	-	-	-	-	-	-	-	-	-	-	-	-

**Fig. 1.** Pathological and medical imaging diagnosis of melanoma. (A) A cutaneous malignant melanoma in a size of 2.5 × 1.5 cm at patient’s right planta and histopathological H&E staining of the needle biopsied melanoma specimen. (B) Representative images of positive IHC staining. Three positive signals of PHH3 are indicated by arrows. Results of IHC examination are summarized in the table. Bars, 250 µm. (C) Whole-body PET/CT scan illustrates irregular focal hypermetabolic activities at the melanoma lesions site (red arrows). Enlarged sentinel lymph nodes (SLNs) with hypermetabolic activities are located at bilateral groins and bilateral iliac blood vessels.

promotes aberrant melanocyte proliferation and initiates tumorigenesis of melanoma [47].

### 3.2. Combined iFISH tumor tissue and liquid biopsies to longitudinally monitor immunotherapeutic efficacy and timely detect cellular MRD

Biphasic iFISH tissue and liquid biopsies were performed throughout full therapy courses. Quantitative iFISH tumor tissue biopsy targeting a variety of tumor markers was respectively carried out on the resected primary tumor, excision margin (Exc Mgn) and dissected SLNs. Recapitulated iFISH biopsies along with diagnosis and treatment are depicted in Fig. 2A. Because the total cell number in different tissue samples varied greatly, the cell density (CD), defined as normalized numbers of detected TCs or TECs per 10,000 cells ( $1 \times 10^4$ ,  $e-4$ ), was utilized to appropriately compare target cell quantities among different iFISH biopsied tissue specimens. As demonstrated in Fig. 2B, (PD-L1, p16)-iFISH tissue biopsy (for Tumor<sup>1</sup> and Exc Mgn<sup>1</sup>) detected 38 TCs (CD,  $69.0e-4$ ) and 3 TECs ( $5.5e-4$ ) among 5510 cells in the resected primary melanoma specimen. Examination of the excision margin sample by the same iFISH analysis showed 30 TCs ( $38.2e-4$ ) and 1 TEC ( $1.3e-4$ ) detected among 7850 cells. All TCs and the TEC were PD-L1<sup>+</sup>. (Ki67, Vim)-iFISH biopsy (for Tumor<sup>2</sup> and Exc Mgn<sup>2</sup>) revealed 35 TCs ( $58.4e-4$ ) and 5 TECs ( $8.3e-4$ ) in 5994 cells of the melanoma specimen. Only one Ki67<sup>+</sup>/Vim<sup>-</sup> null TC was detected in 8915 excision margin cells. (PD-L1, Ki67)-iFISH (for LN1-3<sup>3</sup>) was conducted to examine three dissected SLNs. One PD-L1<sup>+</sup> TEC ( $6.4e-4$ ) out of 1557 cells was detected in SLN-1. Three PD-L1<sup>+</sup> TCs ( $8.4e-4$ ) and 11 PD-L1<sup>+</sup> TECs ( $31.0e-4$ ) were detected in 3553 cells in SLN-3. Zero Ki67<sup>+</sup> TC or TEC was identified in SLN-1 and 3. Neither TC nor TEC was detected in SLN-2.

SE-iFISH liquid biopsy was performed seven times (t1-t7) to longitudinally co-detect CTCs and CTECs expressing diverse tumor markers throughout therapy. Shown in Fig. 2B, when the patient was diagnosed with early-stage melanoma, t1 test showed four non-hematologic circulating aneuploid cells (CACs) including three CD31<sup>-</sup> CTCs and one CD31<sup>+</sup> CTEC in 3 ml of blood. At t2 detection, a pair of SE-iFISH analyses was respectively carried out at t2A and t2B, a week after surgery but before ICI immunotherapy initiation. t2A: (Ki67, Vim)-SE-iFISH liquid biopsy, matching the (Ki67, Vim)-iFISH tissue biopsy<sup>2</sup> on resected melanoma and excision margin specimen, led to comparable investigation of the mutual relevance of traceable subcategorized CTCs vs TCs and CTECs vs TECs. t2B: (PD-L1, NC)-SE-iFISH detected baseline viable and necrotic CTCs and CTECs with their PD-L1 expression status for subsequent monitoring of ICI treatment efficacy. As indicated at t2A, (Ki67, Vim)-SE-iFISH detected seven CACs, including three CTCs and four CTECs. (PD-L1, NC)-SE-iFISH at t2B illustrated the presence of four viable CTCs and two viable CTECs. From t3 (post-cycle-1 of immunotherapy) to t5 (post-cycle-6 treatment), quantities of aneuploid CACs (CTCs + CTECs) steadily persisted during therapy, showing four CTCs at t3 including two necrotic PD-L1<sup>+</sup> and two viable PD-L1<sup>-</sup> cells immediately after one cycle of ICI therapy, three CACs at t4 (2 CTCs and 1 CTEC) and four CACs at t5 (2 CTCs and 2 CTECs). CTC number reduced to one with no detectable CTECs at t6, which was post-cycle-8 or 14 weeks since immunotherapy initiation. Two weeks following entire 12 cycles of ICI treatment, the same pair of SE-iFISH for t2A and t2B tests were conducted to detect cellular MRD at t7. Results exhibited a dramatic increase to 21 CACs (18 CTCs, 3 Ki67<sup>+</sup> CTECs) in the Ki67/Vim category (t7A) and 24 CACs (20 CTCs, 4 CTECs including 1 PD-L1<sup>+</sup> and 3 PD-L1<sup>-</sup> cells) in the PD-L1 category (t7B), suggesting that besides inherent resistance, these specific subtypes of CTCs and CTECs also developed early *de novo* resistance to the ICI agent following full courses of treatment.

### 3.3. In situ phenotypic and karyotypic characterization of iFISH biopsied TCs and TECs in resected melanoma and excision margin tissue

As revealed in Fig. 3A, representative images of iFISH tissue biopsied

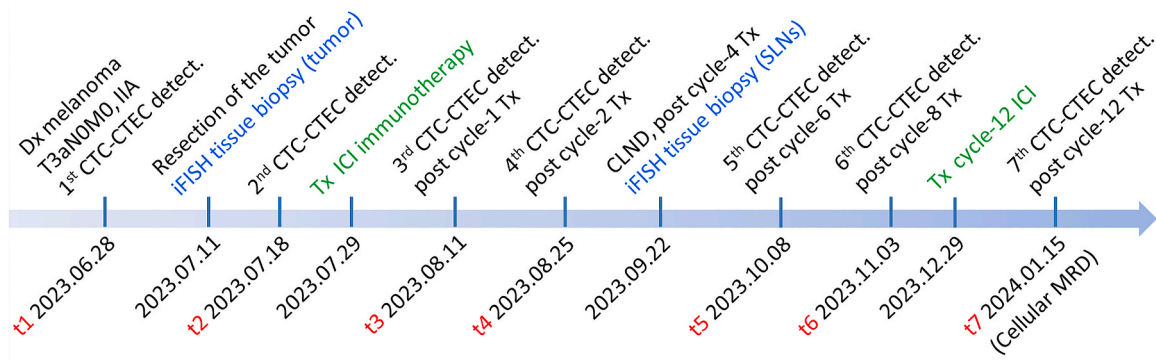
non-hematologic (CD45<sup>-</sup>) TCs and TECs in the resected melanoma, excision margin (Aa-d) and dissected metastatic SLNs (Ae) are respectively demonstrated, including a PD-L1<sup>+</sup>/p16<sup>+</sup>/CD31<sup>-</sup> triploid TC (TC<sup>tri</sup>), a PD-L1<sup>-</sup>/p16<sup>-</sup>/CD31<sup>-</sup> multiploid TC null cell (TC<sup>multi</sup>), a PD-L1<sup>+</sup>/p16<sup>+</sup>/CD31<sup>+</sup> haploid TEC (TEC<sup>mono</sup>), a Ki67<sup>+</sup>/Vim<sup>+</sup>/CD31<sup>+</sup> triploid TEC showing unique cell morphology of Vimentin distribution (TEC<sup>tri</sup>) and a PD-L1<sup>+</sup> haploid TC (TC<sup>mono</sup>). Dramatic difference of the nucleus-to-cytoplasm ratio (N/C ratio) among various TCs and TECs was observed, varying from 0.1 to 0.8.

Distinct Chr8 copy numbers in intact CTCs and CTECs were previously reported to correlate with either intrinsic or *de novo* resistance to chemo- or immunotherapy [36,46]. Accordingly, intact aneuploid CD31<sup>-</sup> TCs and CD31<sup>+</sup> TECs in the current study were prepared from unsliced specimens of melanoma mass, excision margin and metastatic SLNs, followed by systematic analyses of the degree of aneuploidy and diverse tumor marker expression. Two sets of iFISH tumor tissue biopsies respectively targeting PD-L1/p16 and Ki67/Vim were conducted in this study. As illustrated in Fig. 3B, (PD-L1, p16)-iFISH detected a total of 38 TCs and 3 TECs in the resected melanoma tissue sample. Regarding CD31<sup>-</sup> aneuploid TCs, the majority (23 out of 38, 60.5 %) were PD-L1<sup>+</sup>, including 17 PD-L1<sup>+</sup>/p16<sup>-</sup> haploid (17 out of 38, 44.7 %), 1 PD-L1<sup>+</sup>/p16<sup>-</sup> triploid (1 out of 38, 2.6 %), 4 PD-L1<sup>+</sup>/p16<sup>+</sup> double positive haploid (DP, 4 out of 38, 10.5 %) and 1 PD-L1<sup>+</sup>/p16<sup>+</sup> triploid TCs (1 out of 38, 2.6 %). Two TCs were PD-L1<sup>-</sup>/p16<sup>+</sup> triploid cells (2 out of 38, 5.3 %). The remaining 13 TCs were PD-L1<sup>-</sup>/p16<sup>-</sup> double negative null cells (13 out of 38, 34.2 %), including 6 triploid, 4 tetraploid and 3 multiploid null TCs. Among three CD31<sup>+</sup> aneuploid TECs, one was triploid null cell, one was PD-L1<sup>-</sup>/p16<sup>+</sup> haploid and the last was PD-L1<sup>+</sup>/p16<sup>+</sup> haploid cell. In the excision margin sample examined by the same iFISH technique, there were 30 TCs detected with all being PD-L1<sup>+</sup>, including 20 PD-L1<sup>+</sup>/p16<sup>-</sup> haploid (20 out of 30, 66.7 %), 1 PD-L1<sup>+</sup>/p16<sup>-</sup> triploid (1 out of 30, 3.3 %) and 9 PD-L1<sup>+</sup>/p16<sup>+</sup> haploid cells (9 out of 30, 30 %). Only one PD-L1<sup>+</sup>/p16<sup>-</sup> haploid TEC was detected in the excision margin specimen. (Ki67, Vim)-iFISH detected 35 TCs and 5 TECs in the primary tumor mass. Among those TCs, 22 Ki67<sup>+</sup>/Vim<sup>+</sup> haploid (22 out of 35, 62.9 %), 3 Ki67<sup>+</sup>/Vim<sup>+</sup> triploid (3 out of 35, 8.6 %), 1 Ki67<sup>+</sup>/Vim<sup>+</sup> tetraploid (1 out of 35, 2.9 %), 6 Ki67<sup>-</sup>/Vim<sup>-</sup> triploid null (6 out of 35, 17.1 %) and 3 tetraploid null TCs (3 out of 35, 8.6 %) were detected. One Ki67<sup>-</sup>/Vim<sup>-</sup> triploid null TEC was detected in the excision margin specimen.

Altogether, karyotypic analysis demonstrated that haploid cells constituted the major population of TCs in both primary tumor (21 out of 38, 55.3 % for PD-L1 category; 22 out of 35 62.9 % for Ki67 category) and excision margin (29 out of 30, 96.7 % for PD-L1 category), followed by trisomy 8 (10 out of 38, 26.3 % for PD-L1 category; 9 out of 35, 25.7 % for Ki67 category), tetrasomy 8 (4 out of 38, 10.5 % for PD-L1 category; 4 out of 35, 11.4 % for Ki67 category) and  $\geq$ pentasomy 8 (3 out of 38, 7.9 % for PD-L1 category). Primary lesions and the excision margin site in this early-stage melanoma patient had very few TECs, resulting in a high cell density (CD) ratio of TC/TEC = 14 ( $69e-4/5e-4$ ) in the primary tumor and TC/TEC = 38 ( $38e-4/1e-4$ ) in the excision margin sample examined by (PD-L1, p16)-iFISH. Similar to TCs, haploid and triploid cells were the leading populations of TECs in the primary lesions. A significant amount of PD-L1<sup>+</sup> aneuploid TCs and TECs were identified at the excision margin, indicating that the current safety excision margin of 2 cm is still within the area of field cancerization, namely the field cancerized excision margin.

Regarding metastatic SLNs detected by (PD-L1, Ki67)-iFISH (Fig. 3B), LN-1 exhibited 1 TEC ( $6.4e-4$ ) and LN-3 had 11 PD-L1<sup>+</sup>/Ki67<sup>+</sup> haploid TECs ( $31.0e-4$ ) and 3 PD-L1<sup>+</sup>/Ki67<sup>-</sup> haploid TCs ( $8.4e-4$ ). All the TCs and TECs detected in metastatic SLNs were PD-L1<sup>+</sup> haploid cells. Compared to primary tumor and excision margin samples showing a high CD ratio of TC/TEC, LN-3 exhibited a reverse high CD ratio of TEC/TC = 3.7 ( $31.0e-4/8.4e-4$ ). No TCs or TECs were detected in LN-2.

A iFISH tumor tissue and liquid biopsies to longitudinally co-detect TCs-TECs and CTCs-CTECs



B Numerical recapitulation of TCs-TECs and CTCs-CTECs detected at the indicated time intervals

iFISH tissue biopsy to co-detect aneuploid TCs and TECs in resected tumor and dissected lymph node specimens

Tumor <sup>1,a</sup>	69.0e-4 TCs (38 TCs: 18 PD-L1+, 2 p16+, 5 DP, 13 null)	5.5e-4 TECs (3 TECs: 1 p16+, 1 DP, 1 null)
Exc Mgn <sup>1,b</sup>	38.2e-4 TCs (30 TCs: 21 PD-L1+, 9 PD-L1+/p16+ DP)	1.3e-4 TECs (all 1 TEC PD-L1+, 0 p16+)
Tumor <sup>2,c</sup>	58.4e-4 TCs (35 TCs: 26 Vim+, 9 Ki67-/Vim- null)	8.3e-4 TECs (5 TECs: 2 Vim+, 1 DP, 2 null)
Exc Mgn <sup>2,d</sup>	1.1e-4 TCs (1 null)	0 TEC
LN-1 <sup>3,e</sup>	0 TC	6.4e-4 TECs (all 1 TEC PD-L1+)
LN-2 <sup>3,f</sup>	0 TC	0 TEC
LN-3 <sup>3,g</sup>	8.4e-4 TCs (all 3 TCs PD-L1+, 0 Ki67+)	31.0e-4 TECs (all 11 TECs PD-L1+)

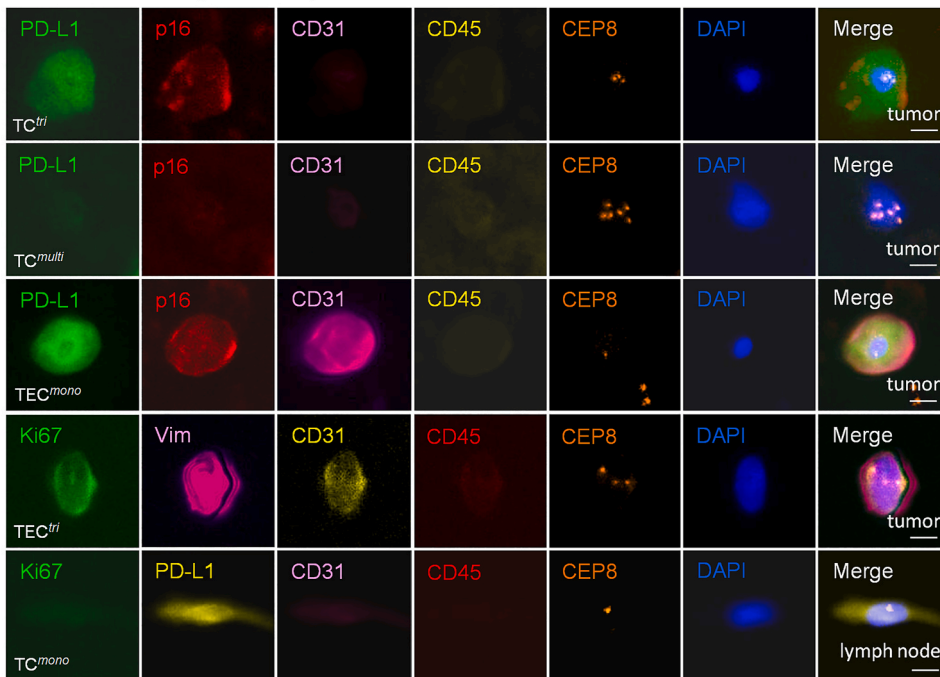
SE-iFISH liquid biopsy to co-detect viable and necrotic PD-L1+ aneuploid CTCs and TECs throughout therapy

t1	SE-iFISH (Vimentin): 4 CACs including 3 CTCs (1 Vim+, 2 Vim-), 1 CTEC (Vim-)
t2	(A) SE-iFISH (Ki67, Vimentin): 7 CACs including 3 CTCs (1 Vim+, 2 null), 4 CTECs (2 Ki67+, 2 null) (B) SE-iFISH (PD-L1, NC): 6 CACs including 4 CTCs (2 viable PD-L1+, 2 viable PD-L1-), 2 CTECs (2 viable PD-L1+)
t3	SE-iFISH (PD-L1, NC): 4 CACs including 4 CTCs (2 necrotic PD-L1+, 2 viable PD-L1-), 0 CTEC
t4	SE-iFISH (PD-L1, NC): 3 CACs including 2 CTCs (2 viable PD-L1-), 1 CTEC (1 viable PD-L1-)
t5	SE-iFISH (PD-L1, NC): 4 CACs including 2 CTCs (2 viable PD-L1-), 2 CTECs (1 viable PD-L1-, 1 viable PD-L1+)
t6	SE-iFISH (PD-L1, NC): 1 CAC including 1 CTC (1 viable PD-L1-), 0 CTEC
t7	(A) SE-iFISH (Ki67, Vimentin): 21 CACs including 18 CTCs (all viable null), 3 CTECs (all viable Ki67+) (MRD) (B) SE-iFISH (PD-L1, NC): 24 CACs including 20 CTCs (all viable PD-L1-), 4 CTECs (1 PD-L1+, 3 viable PD-L1-)

Applied iFISH: iFISH (PD-L1, p16) for Tumor<sup>1</sup> and Exc Mgn<sup>1</sup>; iFISH (Ki67, Vimentin) for Tumor<sup>2</sup> and Exc Mgn<sup>2</sup>; iFISH (PD-L1, Ki67) for LN1-3<sup>3</sup>  
 Total cell numbers in iFISH tissue biopsy: Tumor<sup>a</sup> 5510; Exc Mgn<sup>b</sup> 7850; Tumor<sup>c</sup> 5994; Exc Mgn<sup>d</sup> 8915; LN-1<sup>e</sup> 1557; LN-2<sup>f</sup> 1406; LN-3<sup>g</sup> 3553  
 Dx, Diagnosis; Tx, treatment; LN, lymph node; CLND, complete lymph node dissection; DP, double positive; CAC, circulating aneuploid cell; NC, necrotic cell; Exc Mgn, excision margin

**Fig. 2.** Quantitative recapitulation of combined iFISH tumor tissue and SE-iFISH liquid biopsies. (A) Designated time intervals including diagnosis, iFISH tumor tissue biopsy and SE-iFISH liquid biopsy throughout therapy are depicted in the timeline. (B) Numerical values of target cells detected by combined iFISH biopsies. iFISH tumor tissue biopsy on the primary tumor and the excision margin (Exc Mgn): (PD-L1, p16)-iFISH detects 38 TCs (69.0e-4, normalized target cell numbers per 1 × 10<sup>4</sup> total examined cells) and 3 TECs (5.5e-4) in the resected primary melanoma lesions with a safety excision margin of 2 cm. In the excision margin sample, there are 30 TCs (38.2e-4) and 1 TEC (1.3e-4) detected. (Ki67, Vimentin)-iFISH reveals 35 TCs (58.4e-4) and 5 TECs (8.3e-4) in the primary tumor and only 1 null TC is detected. (PD-L1, Ki67)-iFISH on dissected sentinel lymph nodes shows 1 TEC (6.4e-4) in SLN-1, 3 TCs (8.4e-4) and 11 TECs (31.0e-4) in SLN-3. No TCs or TECs are detected in SLN-2. Time points of SE-iFISH liquid biopsy (3 ml blood): (t1) same time when melanoma is clinically diagnosed, (t2) prior to immunotherapy, (t3-t6) at different time points during therapy and (t7) post-therapy. Numbers of circulating aneuploid cells (CACs) including CD31<sup>-</sup> CTCs and CD31<sup>+</sup> CTECs are indicated in the table. Two necrotic PD-L1<sup>+</sup> CTCs are detected at t3, immediately after one cycle of ICI treatment. Cellular MRD assessment at t7 shows a surge in both CTC and CTEC quantities.

A iFISH tissue biopsied aneuploid TCs and TECs



B Quantitative and molecular characterization of iFISH tissue biopsied tumor and SLNs

	Tumor markers	Haploid		Triploid		Tetraploid		Multiploid		Sum 2	
		tumor	Mgn	tumor	Mgn	tumor	Mgn	tumor	Mgn	tumor	Mgn
CD31 <sup>-</sup> TC (tumor and Exc Mgn)	PD-L1- / p16-	0	0	6	0	4	0	3	0	13	0
	PD-L1+ / p16-	17	20	1	1	0	0	0	0	18	21
	PD-L1- / p16+	0	0	2	0	0	0	0	0	2	0
	PD-L1+ / p16+	4	9	1	0	0	0	0	0	5	9
	Sum 1	21	29	10	1	4	0	3	0	38 (69e-4)	30 (38e-4)
	% (Sum 1/Total)	55%	97%	26%	3%	11%	0	8%	0	(Total)	
	Ki67- / Vimentin-	0	0	6	1	3	0	0	0	9	1
	Ki67+ / Vimentin-	0	0	0	0	0	0	0	0	0	0
	Ki67- / Vimentin+	22	0	3	0	1	0	0	0	26	0
	Ki67+ / Vimentin+	0	0	0	0	0	0	0	0	0	0
Sum 1	22	0	9	1	4	0	0	0	35 (58e-4)	1 (1e-4)	
% (Sum 1/Total)	63%	0	26%	100%	11%	0	0	0	(Total)		
CD31 <sup>+</sup> TEC (tumor and Exc Mgn)	PD-L1- / p16-	0	0	1	0	0	0	0	0	1	0
	PD-L1+ / p16-	0	1	0	0	0	0	0	0	0	1
	PD-L1- / p16+	1	0	0	0	0	0	0	0	1	0
	PD-L1+ / p16+	1	0	0	0	0	0	0	0	1	0
	Sum 1	2	1	1	0	0	0	0	0	3 (5e-4)	1 (1e-4)
	% (Sum 1/Total)	67%	100%	33%	0	0	0	0	0	(Total)	
	Ki67- / Vimentin-	0	0	1	0	1	0	0	0	2	0
	Ki67+ / Vimentin-	0	0	0	0	0	0	0	0	0	0
	Ki67- / Vimentin+	2	0	0	0	0	0	0	0	2	0
	Ki67+ / Vimentin+	0	0	1	0	0	0	0	0	1	0
Sum 1	2	0	2	0	1	0	0	0	5 (8e-4)	0	
% (Sum 1/Total)	40%	0	40%	0	20%	0	0	0	(Total)		
lymph nodes	SLN-1: 1 TEC (6.4e-4); SLN-3: 3 TCs (8.4e-4) and 11 TECs (31.0e-4); SLN-2: none of detectable TC or TEC SLN-3 TEC/TC ratio=3.7 compared to the inverted TC/TEC ratio=14 (tumor), and 38 (Exc Mgn) All TCs and TECs in metastatic SLN-1,3 are PD-L1+ and haploid										

(caption on next page)

**Fig. 3.** Phenotypic and karyotypic profiling of aneuploid TCs and TECs in resected melanoma tissue specimens and dissected sentinel lymph nodes. **(A)** Representative images of iFISH tissue biopsy on the resected primary tumor and excision margin specimens and the metastatic SLN: a PD-L1<sup>+</sup>/p16<sup>+</sup>/CD31<sup>-</sup> triploid TC (PD-L1<sup>+</sup>/p16<sup>+</sup> TC<sup>tri</sup>) with a N/C ratio = 0.1; a PD-L1<sup>-</sup>/p16<sup>-</sup> multiploid TC null cell (null TC<sup>multi</sup>); a PD-L1<sup>+</sup>/p16<sup>+</sup>/CD31<sup>+</sup> haploid TEC (PD-L1<sup>+</sup>/p16<sup>+</sup> TEC<sup>mono</sup>) with a N/C ratio = 0.1; a Ki67<sup>+</sup>/Vim<sup>+</sup>/CD31<sup>+</sup> triploid TEC (Ki67<sup>+</sup>/Vim<sup>+</sup> TEC<sup>tri</sup>) with a unique morphology of Vimentin expression and a N/C ratio = 0.8 and a PD-L1<sup>+</sup> haploid TC (PD-L1<sup>+</sup> TC<sup>mono</sup>) with a N/C ratio = 0.5. Bars, 5 μm. **(B)** Quantitative iFISH tumor tissue biopsy to phenotypically and karyotypically profile aneuploid TCs and TECs in the primary tumor and at the excision margin (exc. mgn.) site. (PD-L1, p16)-iFISH: 38 CD31<sup>-</sup> aneuploid melanoma TCs detected in the resected primary tumor, with a majority (60.5 %) being PD-L1<sup>+</sup> with highly heterogeneous aneuploidy. Two TCs were PD-L1<sup>-</sup>/p16<sup>+</sup> triploid cells. The remaining 13 TCs are PD-L1<sup>-</sup>/p16<sup>-</sup> multiploid null cells. Three CD31<sup>+</sup> aneuploid TECs are PD-L1<sup>-</sup>/p16<sup>-</sup>, PD-L1<sup>-</sup>/p16<sup>+</sup> and PD-L1<sup>+</sup>/p16<sup>+</sup>, respectively. In the excision margin specimen, all 30 detected TCs are PD-L1<sup>+</sup> with 29 out of 30 the haploid cells. (Ki67, Vim)-iFISH detected 35 TCs and 5 TECs in the primary tumor mass. Among those detected TCs with monosomy 8 as the leading ploidy, there are 22 Ki67<sup>-</sup>/Vim<sup>+</sup>, 3 Ki67<sup>+</sup>/Vim<sup>+</sup>, 1 Ki67<sup>-</sup>/Vim<sup>-</sup>, 9 Ki67<sup>+</sup>/Vim<sup>-</sup> null cells. Only one Ki67<sup>-</sup>/Vim<sup>-</sup> null TEC is detected in excision margin sample. Detected by (PD-L1, Ki67)-iFISH, SLN-1 has one TEC (6.4e-4) but no TCs detected; SLN-3 shows 11 TECs (31.0e-4) and 3 TCs (8.4e-4). All detected TCs and TEC in SLN-1 and 3 are PD-L1<sup>+</sup> haploid cells. SLN-2 has no TCs or TECs detected. Compared to the high CD ratio of TC/TEC = 14 in the primary tumor and TC/TEC = 38 in the excision margin specimen, SLN-3 exhibits a reverse high CD ratio of TEC/TC = 3.7.

### 3.4. Comprehensive analysis of SE-iFISH liquid biopsied CTCs and CTECs in blood

Representative images of CTCs and CTECs are revealed in Fig. 4A, including a large Ki67<sup>+</sup>/CD31<sup>+</sup> multiploid CTEC (<sub>1</sub>CTEC<sup>multi</sup>), a large viable PD-L1<sup>+</sup>/CD31<sup>+</sup>/necrotic cell staining (NCS<sup>-</sup>) multiploid CTEC (<sub>1</sub>CTEC<sup>multi</sup>), a small viable PD-L1<sup>+</sup>/CD31<sup>+</sup> triploid CTEC (<sub>3</sub>CTEC<sup>tri</sup>) and a small necrotic PD-L1<sup>+</sup>/CD31<sup>-</sup>/NCS<sup>+</sup> triploid CTC (<sub>3</sub>CTC<sup>tri</sup>). Unlike TCs and TECs possessing a high variety of N/C ratio, almost all spherical CTCs and CTECs exhibited a similar N/C ratio of 0.9, a unified morphology adapted in stressed circulation.

Longitudinal liquid biopsy of total CD31<sup>-</sup> CTCs and CD31<sup>+</sup> CTECs to timely assess ICI efficacy throughout diagnosis and entire therapy courses (t1-t7, Fig. 2B) was graphically depicted in Fig. 4B. SE-iFISH detection at t1 showed three CTCs (one Vim<sup>+</sup> near-diploid, one Vim<sup>-</sup> triploid, one Vim<sup>-</sup> multiploid) and one Vim<sup>-</sup> multiploid CTEC in 3 ml of blood when the patient was diagnosed with early-stage melanoma. (PD-L1, NC)-SE-iFISH (t2B, Fig. 4B) revealed the existence of four viable CTCs (2 PD-L1<sup>+</sup> near-diploid, 1 PD-L1<sup>-</sup> triploid, 1 PD-L1<sup>-</sup> tetraploid) and two viable CTECs (1 PD-L1<sup>+</sup> triploid, 1 PD-L1<sup>+</sup> tetraploid). Serial assessments of ICI therapeutic efficacy by SE-iFISH analyses started from t3 (immediately after one cycle of ICI treatment, Fig. 4B). There were four CTCs detected at t3, consisting of two necrotic PD-L1<sup>+</sup> near-diploid and two viable PD-L1<sup>-</sup> triploid CTCs. No CTECs were detected at t3. Detection at t4 showed two viable PD-L1<sup>-</sup> triploid CTCs and one viable PD-L1<sup>-</sup> multiploid CTEC. Testing at t5 detected one viable PD-L1<sup>-</sup> triploid CTC, one viable PD-L1<sup>-</sup> tetraploid CTC, one viable PD-L1<sup>-</sup> multiploid CTEC and one viable PD-L1<sup>+</sup> multiploid CTEC. A distinct decline to one viable PD-L1<sup>-</sup> multiploid CTC was observed at t6. (PD-L1, NC)-SE-iFISH at t7B detected a surge of MRD CACs containing 20 PD-L1<sup>-</sup> CTCs (6 triploid, 5 tetraploid, 9 multiploid cells), 1 PD-L1<sup>+</sup> multiploid CTEC and 3 PD-L1<sup>-</sup> multiploid CTECs (Fig. 4B). The percentage of PD-L1<sup>+</sup> CTECs among total MRD CTECs was 25 % (1 out of 4 cells). Revealed in Fig. 4B, the same (Ki67, Vim)-SE-iFISH utilized at pretreatment t2A detection was applied at t7A to assess cellular MRD. At t2A, three CTCs (1 Ki67<sup>+</sup>/Vim<sup>+</sup> near-diploid, 1 triploid null, 1 multiploid null) and four CTECs (2 Ki67<sup>+</sup>/Vim<sup>-</sup> multiploid, 2 multiploid null cells) were detected while t7A displayed a surge to 18 Ki67<sup>+</sup>/Vim<sup>-</sup> null CTCs (6 triploid, 1 tetra, 11 multiploid cells) and three Ki67<sup>+</sup>/Vim<sup>-</sup> multiploid CTECs at. As demonstrated in Fig. 4B, PD-L1<sup>+</sup> CTCs had been eliminated from t4. However, MRD assessment at t7(A,B) detected one PD-L1<sup>+</sup> and three Ki67<sup>+</sup> CTECs as well as a large number of Ki67<sup>+</sup>/Vim<sup>-</sup> CTC null cells. In contrast to melanoma PD-L1<sup>+</sup> CTCs being responsive to ICI, PD-L1<sup>+</sup> CTECs exhibited resistance to ICI treatment. Similarly, multiploid (≥pentasomy 8) PD-L1<sup>+</sup> CTECs in advanced NSCLC patients were also found to be inherently resistant to the ICI-nivolumab, whereas triploid PD-L1<sup>+</sup> CTECs developed *de novo* resistance to the same agent [36].

It has been reported that small and large cell sized gastric CTCs respectively exhibited different mechanisms of therapeutic resistance [48], suggesting that cell morphology associates with distinct clinical utilities. In the current study, all CACs (t1-t7) including CTCs and CTECs were karyotypically and morphologically analyzed and summarized in

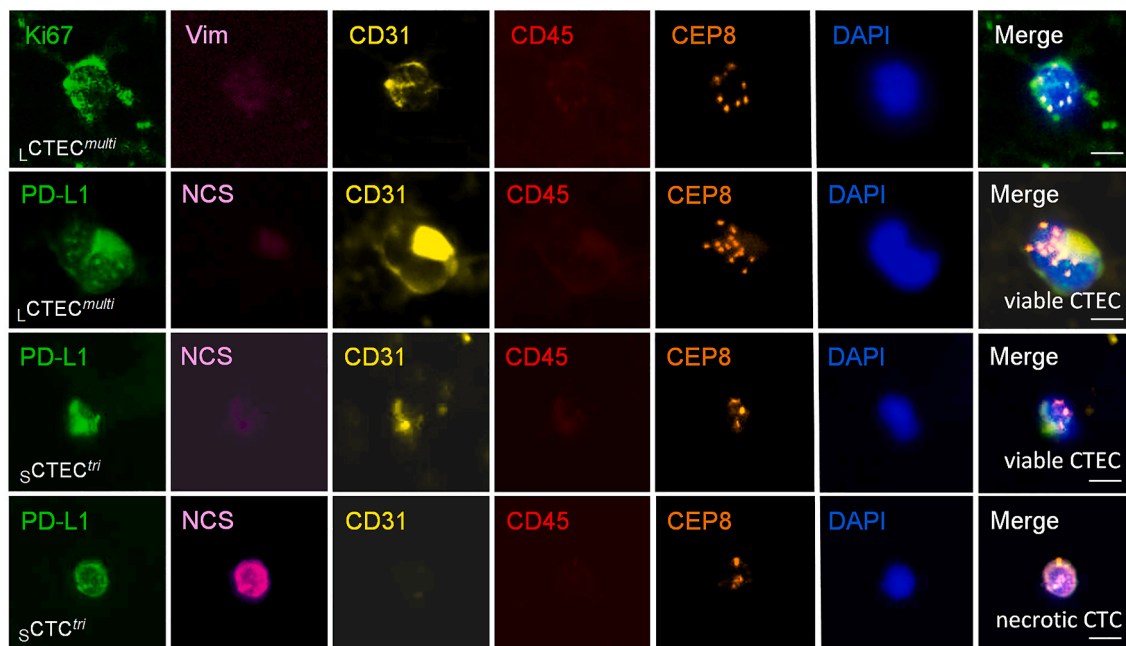
Fig. 4C. Among a total of 74 detected melanoma CACs, 57 were CTCs (57 out of 74, 77.0 %) and 17 were CTECs (17 out of 74, 23.0 %), contrasting to the high amount and ratio of CTECs to CTCs detected in NSCLC patients subjected to bevacizumab [37]. CTCs were highly heterogeneous in both Chr8 ploidy and cell morphology. Among the 57 detected CTCs, multiploid large cells (23 out of 57, 40.4 %) and triploid small cells (16 out of 57, 28.1 %) were the main populations, with the remainder being small near-diploid cells (6 out of 57, 10.5 %), large tetraploid cells (4 out of 57, 7.0 %), small tetraploid cells (4 out of 57, 7.0 %) and large triploid cells (4 out of 57, 7.0 %). Regarding 17 CTECs, most were large multiploid cells (15 out of 17, 88.2 %), with the exception of one small triploid and one tetraploid cell (1 out of 17, 5.9 %).

### 3.5. Stratified molecular profiling of mutually relevant subcategorized TCs, TECs, CTCs and CTECs in the therapeutically stressed metastatic cascade

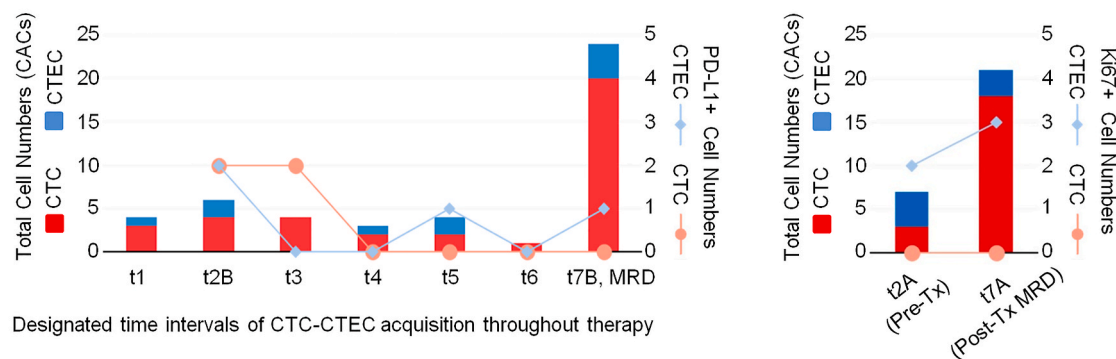
As revealed in Fig. 5, stratified molecular profiling of diverse subtypes of target cells expressing melanoma prognostic markers in both resected specimens and cellular components in blood, along the axis of ICI pretreatment-during treatment-posttreatment, was graphically mapped and analyzed to show how target cells distribute during tumor progression and metastatically relate to each other alongside therapy. As shown in Fig. 5A, (Ki67, Vimentin)-iFISH tumor tissue and liquid biopsies were applied at t2A to respectively examine TCs/TECs in the resected tumor lesions and CTCs/CTECs in blood prior to ICI therapy. As depicted in Figs. 3 and 5A, among the 40 aneuploid cells detected in the melanoma tissue specimen, 35 were TCs (87.5 %) and 5 were TECs (12.5 %) in the Ki67-Vimentin category. Among the 35 TCs and 5 TECs, 26 TCs were Ki67<sup>+</sup>/Vim<sup>+</sup> (26 out of 35, 74.3 %), 1 TEC was Ki67<sup>+</sup>/Vim<sup>+</sup> (1 out of 5, 20 %) and 2 TECs were Ki67<sup>-</sup>/Vim<sup>+</sup>. A total of three TECs were Ki67<sup>+</sup>/Vim<sup>+</sup> double positive cells (3 out of 5, 60 %). Chr8 copy number analysis indicated that there were 22 TCs with monosomy 8 (22 out of 35, 62.9 %), 9 with trisomy 8 (9 out of 35, 25.7 %) and 4 with tetrasomy 8 (4 out of 35, 11.4 %). As illustrated in Fig. 5A, (Ki67, Vimentin)-SE-iFISH liquid biopsy at t2A detected seven CACs containing three CD31<sup>-</sup> CTCs (3 out of 7, 42.9 %) and four CD31<sup>+</sup> CTECs (4 out of 7, 57.1 %). The three CTCs were respectively Ki67<sup>+</sup>/Vim<sup>+</sup> near-diploid (1 out of 3, 33.3 %), triploid Ki67<sup>-</sup>/Vim<sup>-</sup> null (33.3 %) and multiploid null cell (33.3 %), whereas all four CTECs were multiploid with two being Ki67<sup>+</sup>/Vim<sup>-</sup>. Among detected CTCs, 33 % were large cells and 67 % were small size (≤5 μm), whereas all CTECs were multiploid large cells. Co-existence of Ki67<sup>+</sup> TECs and Vim<sup>+</sup> TCs in the primary tumor with their counterpart Ki67<sup>+</sup> CTECs and Vim<sup>+</sup> CTCs in blood inferred metastatic interplay among those cells.

In addition to single point (t2A) comparison with the Ki67-Vimentin category of cells, longitudinal multi-point detection of TCs, TECs, CTCs and CTECs in the PD-L1 category (t2B-t6) was performed and depicted in Fig. 5B. Several metastasis and immunotherapy-related indexes including the percentage of TCs vs TECs, PD-L1 expression, degrees of aneuploidy and cell morphology were comprehensively analyzed to investigate distribution, relevance and subtype transition among those

A SE-iFISH liquid biopsied viable and necrotic aneuploid CTCs and CTECs



B Quantification of subcategorized CTCs and CTECs to timely evaluate therapeutic efficacy



C Karyotypic and morphological characterization of overall aneuploid CTCs and CTECs (t1-t7)

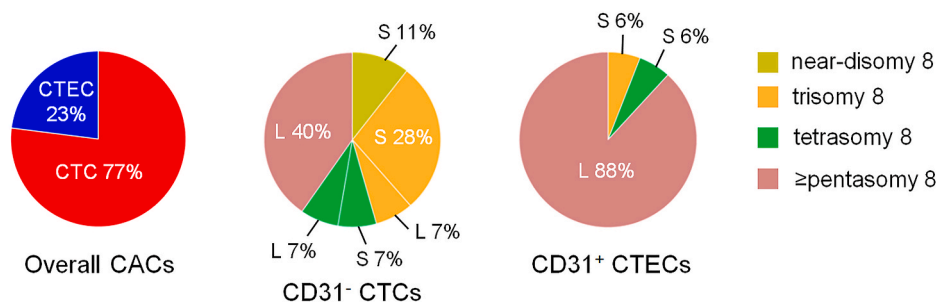


**Fig. 4.** Molecular quantification and profiling of SE-iFISH liquid biopsied aneuploid CTCs and CTECs. **(A)** Representative images of SE-iFISH liquid biopsied CTCs and CTECs. A large Ki67<sup>+</sup>/CD31<sup>+</sup> multiploid CTEC (Ki67<sup>+</sup> LCTEC<sup>multi</sup>); a large viable PD-L1<sup>+</sup>/CD31<sup>+</sup>/NCS<sup>-</sup> multiploid CTEC (PD-L1<sup>+</sup> LCTEC<sup>multi</sup>); a small viable PD-L1<sup>+</sup>/CD31<sup>+</sup> triploid CTEC (PD-L1<sup>+</sup> sCTEC<sup>tri</sup>); a small necrotic PD-L1<sup>+</sup>/CD31<sup>-</sup>/necrotic cell staining (NCS)<sup>+</sup> triploid CTC (PD-L1<sup>+</sup> sCTC<sup>tri</sup>). Almost all spherical CTCs and CTECs exhibit a unified N/C ratio of 0.9. Bars, 5 μm. **(B)** Longitudinal detection of CTCs and CTECs (3 ml blood/specimen) throughout therapy is graphically depicted in Ba. Following ICI administered, PD-L1<sup>+</sup> CTCs are eradicated from t4. PD-L1<sup>+</sup> CTECs are constantly detected at t5 and t7. Large quantity of CTCs in conjunction with one PD-L1<sup>+</sup> CTEC at t7B and three Ki67<sup>+</sup> CTECs at t7A are revealed by cellular MRD assessment (t7). **(C)** Karyotypic and morphological analyses of overall detected CTCs and CTECs (t1-t7). A total of 74 CACs are detected (t1-t7) containing 57 CTCs (57 out of 74, 77.0%) and 17 CTECs (17 out of 74, 23%). Large (L) multiploid (23 out of 57, 40%) and small (S) triploid (16 out of 57, 28%) cells are the main populations of CTCs. Most CTECs are large multiploid cells (15 out of 17, 88%).

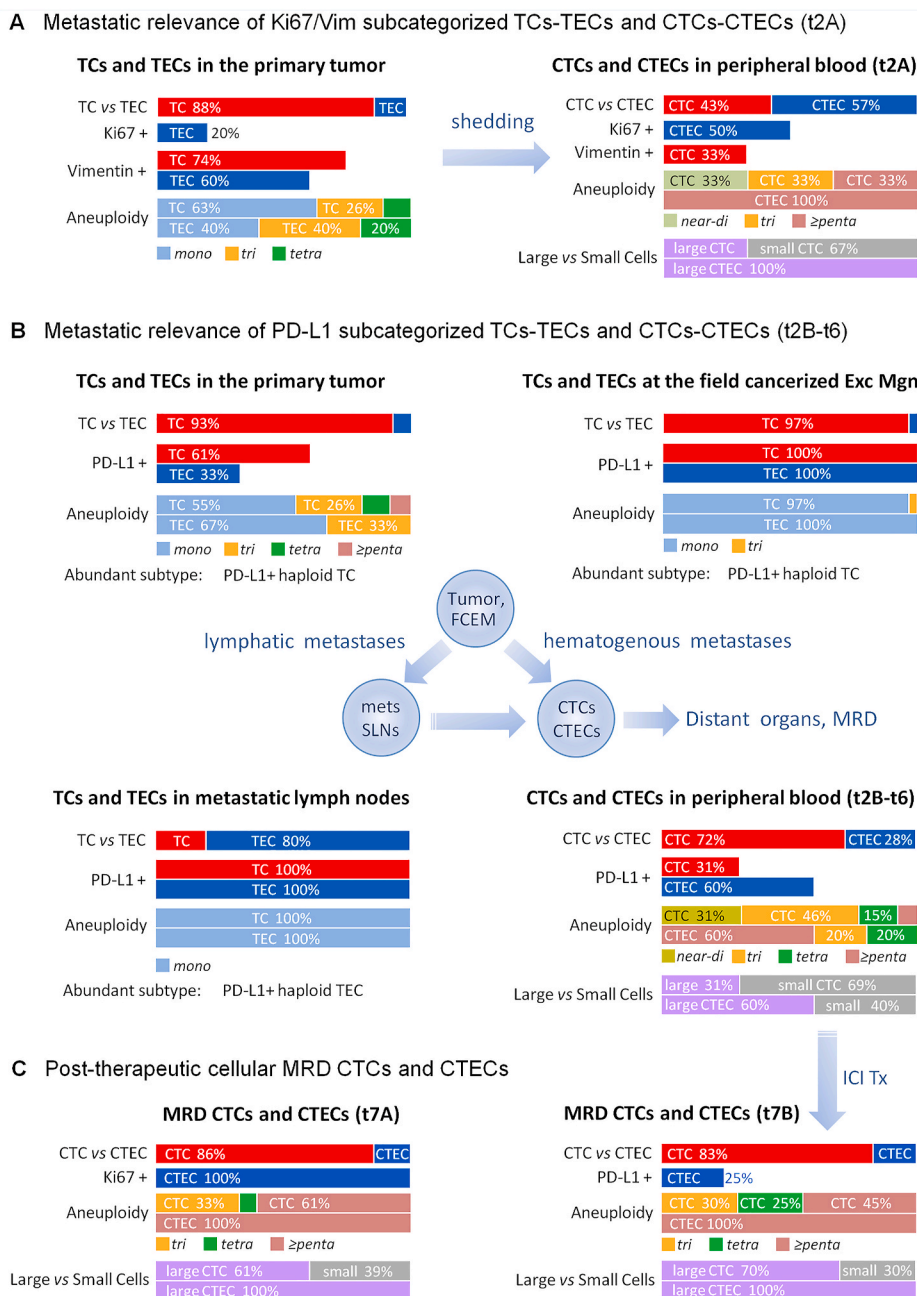


**Fig. 5.** Stratified molecular profiling and mapping of mutually relevant subcategorized TCs-TECs and CTCs-CTECs in therapeutically stressed lymphatic and hematogenous metastatic cascades. Quantified indexes are expressed in percentage. (A) Pre-ICI treatment (quantification analysis of Ki67-Vimentin category of cells): (Ki67, Vimentin)-iFISH tissue biopsy on the resected primary tumor and (Ki67, Vimentin)-SE-iFISH liquid biopsy on blood specimens at t2A are illustrated. Ki67<sup>+</sup> TECs and Vim<sup>+</sup> TCs in the primary tumor are co-detected with their counterpart Ki67<sup>+</sup> CTECs and Vim<sup>+</sup> CTCs in blood, suggesting Ki67<sup>+</sup> TECs and Vim<sup>+</sup> TCs may possess high potential for hematogenous metastases. (B) Pre- and during ICI treatment (analysis of PD-L1 category of cells): (PD-L1, p16)-iFISH tissue biopsy shows a high TC/TEC ratio in the primary melanoma and at the field cancerized excision margin (FCEM) prior to ICI therapy. However, there is a reversed high ratio of TEC/TC in metastatic sentinel lymph nodes (SLNs) following initiation of ICI treatment. TCs and TECs at the excision margin and in metastatic SLNs share a similar phenotypic PD-L1 expression and karyotypic monosomy 8. TCs-TECs in the primary lesions and CTCs-CTECs in blood (t2B-t6) display highly heterogeneous aneuploidy, indicating potential metastatic correlations between the primary tumor and CTCs-CTECs, as well as the interrelationship between the field cancerized excision margin and metastatic SLNs. (C) Post-therapeutic cellular MRD CTCs and CTECs analysis: comparing pre-treatment CTCs and CTECs at t2A with MRD cells at t7A, MRD cells displayed an increased proportion of CTCs (86 %) and large cell CTCs (61 %). Ki67<sup>+</sup> multiploid CTECs are constantly detected from pre-treatment to MRD. Dynamic progression of CTCs and CTECs along the treatment-MRD axis are analyzed by comparing CTCs and CTECs (t2B-t6) with MRD cells (t7B), showing an increased proportion of large CTCs (70 %). All detected CTECs are multiploid large cells. No PD-L1<sup>+</sup> CTCs, near-diploid CTCs, triploid or tetraploid CTECs are detected in MRD cells.

diverse subtypes of cells during the therapeutically stressed dynamic metastasizing process and therapy-resistant cellular MRD development. Compared to the high proportion of CD31<sup>+</sup> TCs in the primary tumor (38 out of 41, 93 %, Fig. 5B) and field cancerized excision margin (FCEM, 30

out of 31, 97 %, Fig. 5B) specimens, the proportion of TCs in metastatic SLN-1 and 3 was only 20 % (3 out of 15, 20 %, Figs. 1 and 5B), with remaining aneuploid cells in dissected SLNs being CD31<sup>+</sup> aneuploid TECs (12 out of 15, 80 %, Fig. 5B). The opposite TC/TEC ratio between

metastatic SLNs and tumor mass was consistent with CD ratio analysis. In peripheral blood, the CTC/CTEC ratio (77%/23% = 3.4, Fig. 5B) was similar to that observed in the primary tumor and excision margin. Concerning PD-L1 expression, 60.5% TCs (23 out of 38 total TCs, Figs. 5B) and 33.3% TECs (1 out of 3 total TECs, Fig. 5B) in melanoma lesions were PD-L1<sup>+</sup> and all TCs and TECs in both field cancerized excision margin sample and metastatic SLNs were PD-L1<sup>+</sup> (Fig. 5B). Regarding PD-L1 expression on CTCs and CTECs in the same category of cells including pre-ICI (t2B) and during ICI therapy (t3-t6, Figs. 2), 13 CTCs and 5 CTECs were detected. Among those detected cells, four CTCs (4 out of 13, 30.8%) and three CTECs (3 out of 5, 60.0%) were PD-L1<sup>+</sup> (Fig. 5B).

Highly heterogeneous aneuploidies in TCs, ranging from haploid to multiploid ( $\geq$ pentasomy 8), were detected in the resected melanoma specimen. As demonstrated in Fig. 5B, the majority of aneuploid cells' population in primary lesions were haploid TCs (55%) and TECs (67%), followed by triploid TCs (26%) and TECs (33%). Almost all TCs and TECs in the field cancerized excision margin specimen and metastatic SLNs were haploid cells except for one TC in the FCEM being triploid (Fig. 5B). PD-L1<sup>+</sup> haploid TCs were the most abundant subtype of cells in both primary melanoma and the excision margin, whereas PD-L1<sup>+</sup> haploid TECs were the most representative subtype of cells in metastatic SLNs, suggesting that TECs in the primary tumor and excision margin area may possess a high lymphatic metastasis potential to SLNs.

Resistance to ICI immunotherapy following cycle-12 treatment completion was observed in this study. Comparing pre-treatment CTCs and CTECs at t2A (Fig. 5A) with MRD cells at t7A (Fig. 5C), the latter displayed an increased proportion of CTCs from 43% to 86% and large cell CTCs from 33% to 61%. Moreover, large Ki67<sup>+</sup> multiploid CTECs were persistently detected from pre-treatment to MRD (Figs. 4B and 5C). Dynamic variation and/or progression of CTCs and CTECs along the treatment-MRD axis were analyzed in Fig. 5B and C, showing that, in comparison with the PD-L1 category of CTCs and CTECs detected during therapy, post-therapeutic viable MRD cells (t7B) exhibited an increased proportion of large CTCs from 31% to 70% and large CTECs from 60% to 100% as well as an increased percentage of multiploidy in CTECs from 60% to 100%.

#### 4. Discussion

Considerable efforts have been made in an attempt to effectively manage malignant melanoma cells with aberrant cytogenetic aneuploidy more effectively. Since Li and colleagues' initial discovery in 2014 demonstrating that trisomy 8 or  $\geq$  pentasomy 8 in SE-iFISH-identified CTCs was respectively correlated with either inherent or *de novo* resistance to the chemotherapeutic agent cisplatin in gastric cancer patients [46], several additional studies on diverse types of cancers further supported that CTCs and CTECs bearing different degrees of aneuploidy were correlated with distinct clinical utilities [23,36,37,42], indicating the necessity to precisely quantify entire aneuploid chromosomes in intact neoplastic cells in both peripheral blood and primary tumor tissue. However, traditional pathology biopsy performed on ultra-thin sliced, paraffin-embedded tumor tissues may lose intact cell nuclei and complete chromosomal contents, resulting in unreliable FISH detection of entire chromosomal aneuploidy in cells. In this study, unlike conventional pathology biopsy, the optimized iFISH tumor tissue and liquid biopsies were applied to co-detect intact melanoma TCs and TECs containing entire chromosomes in unsliced tumor tissue and peripheral blood specimens, enabling *in situ* phenotypic and karyotypic profiling of subcategorized target cells, including TCs, TECs, CTCs and CTECs in the primary tumor, field cancerized excision margin region, SLNs and peripheral blood to effectively probe the optimal safety excision margin, explicitly diagnose metastatic SLNs and provide the rationale for administering immunotherapy. Combined biphasic co-detection of these target cells located at different sites provides a novel full-scale landscape regarding how those target cells are

metastatically related to each other during therapeutically stressed tumor progression and lymphatic/hematogenous metastases.

Surgical resection is commonly the first choice for eligible subjects with stage I-IIIB melanoma [2]. Excision margin has profound impact on post-surgical MRD tumor cells and post-operative recurrence. Currently, the defined safety excision margin for melanoma resection is 2 cm [9]. In the present study, a significant amount of PD-L1<sup>+</sup> aneuploid TCs with a tumor cell density (CD) of 38e-4 was detected at the conventional safety excision margin (Fig. 6B) compared to the primary melanoma with a CD value of 69e-4 (Fig. 3B). Our recent examination on patients with cutaneous squamous cell carcinoma, basal cell carcinoma and other types of cancers, such as glioma and hepatocellular carcinoma (HCC), etc., showed that numerous aneuploid TCs and TECs could also be detected at the excision margin, or at an extended EM even at 4 cm in some skin cancer patients, indicating that outstretched field cancerization, namely the distant FC [12], could reach an area as far as double the current safety excision margin (Fig. 6A). It has been reported that field cancerized cells share similar genomic contents with cancer cells at the primary site. However, these field cancerized cells exhibit normal cell morphology that cannot be identified by conventional histopathology biopsy, thus making molecular characterization, such as aneuploidy examination, a more reliable approach for detecting field cancerized cells [12]. Integrated phenotypic and karyotypic biopsy performed by iFISH in this study was confirmed to be able to effectively detect aneuploid field cancerized cells, thus enabling precise definition of field cancerization region.

The risk of field cancerization in postsurgical recurrence has been underestimated [11,12,49]. Given that increased postoperative relapse-relevant cellular MRD aneuploid CTCs and CTECs could also be detected in many patients with different types of cancers, such as glioma [50], lung [51], pancreatic [52] and HCC [53], several pivotal questions are worthy of further extensive investigation: whether field cancerized cells beyond the conventional safety excision margin contribute to post-surgical MRD CTCs and CTECs, how to more objectively specify the optimal safety excision margin based on the precisely and quantitatively delineated field cancerization region, how to define the risk threshold according to either the CD cut-off values which varies from single to quadruple-digit numbers of TCs and/or TECs normalized to per 10,000 (e-4) total examined cells, or the ratio of either TCs or TECs expressing the cell proliferation marker Ki67 vs TCs or TECs expressing the tumor suppressor marker p16 and how the newly defined risk threshold-based safety excision margin correlates with post-surgical recurrence.

An early and explicit diagnosis of metastatic SLNs followed by CLND has particular clinical values in terms of time-dependent benefits to melanoma patients' survival [7,8]. Richtig and colleagues reported that positive SLNB was lower than 9.1% when biopsy was performed within 43 days following the primary melanoma diagnosis, yet all SLNB were positive when biopsied more than 80 days after the initial diagnosis [8]. The patient in this study had several enlarged SLNs with hypermetabolic activities, initially diagnosed with benign inflammatory hyperplasia. Considering the constant presence of CTCs and CTECs since ICI therapy started, enlarged SLNs were preventively dissected 85 days after melanoma was diagnosed. iFISH tissue biopsy detected PD-L1<sup>+</sup> aneuploid TCs and TECs in two of three examined SLNs with TC density of 8.4e-4 and TEC density of 31.0e-4, indicating SLNB positive with early metastases in biopsied SLNs. Of particular interest is that, compared to a high ratio of TC/TEC = 14 and 38 respectively in the primary tumor and the excision margin specimens, LN-3 had a reverse ratio of TEC/TC = 3.7 in this early-stage subject (Fig. 3B/5B). This contrasted to the late-stage melanoma patient recruited in a different study, showing a large amount of aneuploid TCs (162.0e-4, 250.9e-4) but no TECs detected in a total of two iFISH biopsied SLNs. A significantly high ratio of TECs over TCs in this patient's SLNs suggests that TECs may play a critical role in early lymphatic metastasis. As depicted in Fig. 5B, it is important to note that although the inverse ratio of TC/TEC was observed between the excision margin and metastatic SLNs, almost all TCs and TECs detected at the

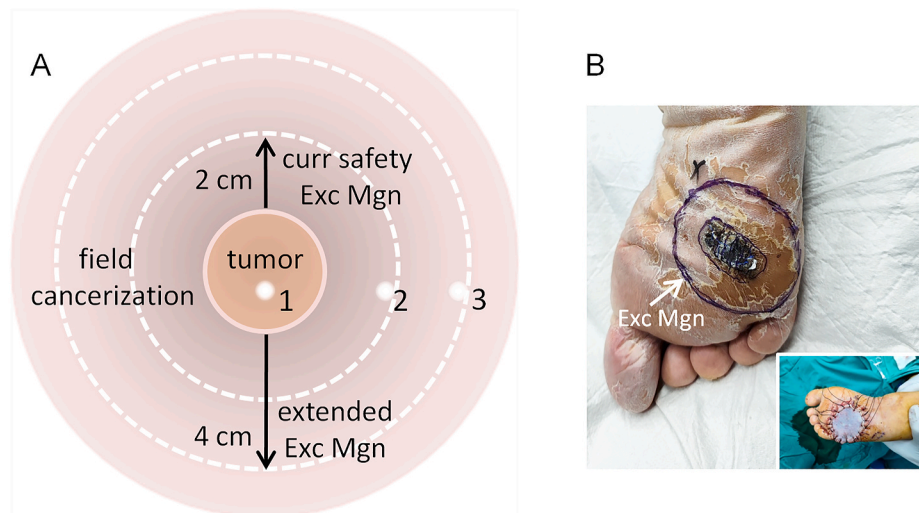


**Fig. 6.** Field cancerized excision margin. (A) Schematic diagram of the field cancerized excision margin is depicted. Primary cutaneous tumor and the current safety excision margin for melanoma (2 cm, white dotted line) as well as the extended excision margin (4 cm, white dotted line) in the area of field cancerization (brown) are depicted. Locations of sample collection in the melanoma tumor mass and at the site of the excision margin (2 cm) for iFISH tissue biopsy in this study are indicated by white dot-1 and 2, respectively. Sampling location at the extended excision margin (4 cm) for iFISH biopsied cutaneous squamous cell carcinoma and basal cell carcinoma is marked by dot-3. (B) The conventional safety excision margin (2 cm) of the surgical resection performed on the patient in this study.

excision margin and in SLNs were homogeneously PD-L1<sup>+</sup> haploid cells. Potential implications of those distinctions among different locations and stages warrant further investigation. Obtained results, being consistent with that previously reported by others [8], demonstrated that integrated phenotypic and karyotypic biopsy is able to quantitatively diagnose early metastasis in SLNs.

ICI is regarded as one of the most effective regimens for metastatic melanoma and other different types of cancers [1,2,54]. Conventional histopathological tumor tissue biopsy snapshots PD-L1 status only once in the IFN $\gamma$ -activated T cells infiltrated spot, rendering non-prognostic value and potential nonnegligible false negative detection [55]. Conversely, detection of PD-L1 on CTCs enables longitudinal assessment of dynamic PD-L1 expression in real-time. Phenotypic expression of PD-L1 and other tumor markers (such as HER2) on CTCs does not necessarily match that of TCs hosted in tumor lesions [23,36,56]. However, concordant positive detection of PD-L1 on both TCs and CTCs allows for predicting response to ICI with 100 % accuracy in advanced melanoma [57]. The melanoma patient in this study demonstrated that PD-L1 was profoundly expressed on the majority of pre-treatment TCs, TECs, CTCs and CTECs located at different examined sites, including primary tumor, excision margin, metastatic SLNs and peripheral blood, leading to the rationale of administering ICI immunotherapy. The quantity of CTCs declined to one cell with no detectable CTECs at t6, indicating an initial favorable response to ICI. However, this patient also exhibited a viable PD-L1<sup>+</sup> CTEC during treatment at t5 (Fig. 2B). Association of detectable post-therapeutic PD-L1<sup>+</sup> cells with poor outcomes in melanoma patients was reported by others [57,58]. Moreover, this subject also exhibited a Q61K activation mutation in the *NRAS* gene, conferring constitutive MAPK and PI3K signaling that facilitates cell proliferation and invasiveness in aberrant melanocytes [47]. Such mutation, in combination with several unfavorable indexes including residual PD-L1<sup>+</sup> TCs and TECs in the field cancerization area beyond excision margin, iFISH biopsied target cells possessing a high N/C ratio (Fig. 3A) [59] and high degrees of aneuploidy [22], positive detection of a series of inferior prognosis-relevant cells, including post-therapeutic PD-L1<sup>+</sup> CTECs, aggressive melanoma-associated mesenchymal marker Vimentin<sup>+</sup> TCs and CTCs [28], cell proliferation marker Ki67<sup>+</sup> TECs and CTECs [27] and necrotic CTCs as few as only once following one cycle of ICI therapy at t3 (Fig. 2B), all suggested that the subject might exhibit poor outcomes.

Comprehensive analyses of ICI-resistant cells showed that small quantity of PD-L1<sup>-</sup> null CTCs were constantly detected throughout immunotherapy (t3-t6, Fig. 2), indicating that those cells might be inherently resistant to ICI treatment. Cellular MRD assessment at t7 revealed a dramatic surge of null CTCs and diverse subtypes of CTECs. Among those MRD CTCs and CTECs, an increased proportion of tetraploid (from 15 % to 25 %) and multiploid (from 8 % to 45 %) large cell sized CTCs as well as large multiploid Ki67<sup>+</sup> or PD-L1<sup>+</sup> CTECs were observed (Fig. 5B), suggesting that newly arisen subtypes of CTCs and CTECs at t7 might develop early *de novo* resistance to ICI-sensitized immune T cells' attack. This keeps in accordance with previously reported existence of immunosuppressive TECs [31]. Regarding ICI-sensitive cells, vanishment of PD-L1<sup>+</sup> near-diploid CTCs and triploid/tetraploid CTECs following treatment (t2-t6) indicated that those specific subtypes of target cells were more sensitive to ICI therapy. Opposite ICI effectiveness between melanoma PD-L1<sup>+</sup> CTECs and PD-L1<sup>+</sup> CTCs in this study is consistent with previously reported NSCLC PD-L1<sup>+</sup> CTECs being resistant to the ICI agent nivolumab but PD-L1<sup>+</sup> CTCs being responsive to the same agent [36].

In addition to PD-L1, the cell proliferation marker Ki67 and the mesenchymal indicator Vimentin also function as effective prognosticators for melanoma [27,28,57,60,61]. To outline detected melanoma cells expressing these prognostic markers at different stages and locations, summarized phenotypic comparison is illustrated in Fig. 7. Vimentin was profoundly expressed in TCs, TECs and CTCs whereas Ki67 was exclusively detected in TECs and their counterpart CTECs. This was disparate from expression of Ki67 being observed only in CTCs in the rare cutaneous Merkel cell carcinoma patient [62]. Moreover, all detected TCs and TECs at the excision margin and in metastatic SLNs were PD-L1<sup>+</sup> (100 %) and about 60 % of TCs in the primary tumor or CTECs in blood were PD-L1<sup>+</sup>. When ICI-resistant MRD developed, PD-L1<sup>+</sup> CTECs and Ki67<sup>+</sup> CTECs (100 %) were detected. Taken together, TECs and CTECs respectively expressing PD-L1 and Ki67 were the only cell types observed in both primary tumor and peripheral blood as well as at MRD assessment. Critical roles of diverse subtypes of TECs and CTECs in tumor progression and ICI-resistance are particularly worthy of further in-depth investigation.

Pinpointing what subtypes of TCs and TECs in the primary tumor possess high metastasizing potential and illustrating how diverse subtypes of TCs, TECs, CTCs and CTECs are related to each other in

Classification	Primary Tumor		Excision Margin		Metastatic SLNs		Blood (t2A)		Blood (t2B-t6)		Blood (t7A, MRD)		Blood (t7B, MRD)	
	TCs	TECs	TCs	TECs	TCs	TECs	CTCs	CTECs	CTCs	CTECs	CTCs	CTECs	CTCs	CTECs
PD-L1+	60.5% (23/38)	33.3% (1/3)	100% (30/30)	100% (1/1)	100% (3/3)	100% (12/12)	/	/	30.8% (4/13)	60.0% (3/5)	/	/	0%	25.0% (1/4)
Ki67+	0%	20.0% (1/5)	/	/	/	/	0%	50.0% (2/4)	/	/	0%	100% (3/3)	/	/
Vimentin+	74.3% (26/35)	60.0% (3/5)	/	/	/	/	33.3% (1/3)	0%	/	/	0%	0%	/	/

**Fig. 7.** Phenotypic comparison of melanoma index-relevant prognostic markers expressed on aneuploid target cells at different stages and locations. All detected TCs and TECs (100 %) at the excision margin and in metastatic SLNs are PD-L1<sup>+</sup>. The majority of TCs (61 %) and CTECs (60 %) in the primary tumor and circulation, respectively, have PD-L1 expression. Only PD-L1<sup>+</sup> CTECs (25 %) and Ki67<sup>+</sup> CTECs (100 %) are detected when ICI-resistant MRD developed.

lymphatic and hematogenous metastatic cascades remain highly challenging. In this early-stage melanoma patient, PD-L1<sup>+</sup> haploid TECs existed in the primary tumor foci, field cancerized excision margin region and metastatic SLNs (Fig. 5B), implying that this specific subtype of TECs may function as the primary contributor in lymphatic metastases. Involvement of TECs in early-stage melanoma metastasis is of particular concern. Regarding hematogenous metastases, provided that Ki67<sup>+</sup> TECs and Vim<sup>+</sup> TCs in the primary tumor were respectively co-detected with their counterparts Ki67<sup>+</sup> CTECs and Vim<sup>+</sup> CTCs in blood (t2A in Figs. 5A and 7), it is rational to reason that specific subtypes of Ki67<sup>+</sup> TECs and Vim<sup>+</sup> TCs in the primary tumor may possess a high potential for hematogenous metastases. Additional correlation analysis indicated that TCs possessing trisomy 8, tetrasomy 8 and ≥pentasomy 8 in the primary lesions may relate to CTCs bearing the same matched heteroploidies of Chr8 (Fig. 5B). Conversely, triploid and tetraploid TECs in the primary tumor and multiploid TECs in the excision margin area may be respectively related to their counterpart CTECs carrying the same matched aneuploidy in peripheral blood (Fig. 5B). Further karyotypic analysis in Fig. 5B indicated that compared to TCs and TECs in the primary tumor, a newly arisen multiploidy (≥pentasomy 8) was identified in CTCs and CTECs. One of possibilities that such *de novo* ploidy might potentially originate from adapted evolution of post-therapeutic karyotype shifting in stressed circulation cannot be ruled out [20,21].

It is of crucial importance to precisely monitor and further investigate phenotype and karyotype shifting in CTCs and CTECs throughout therapy, particularly when treatment-resistance emerges either during or following completion of treatment. Fig. 5 illustrates the distribution and traceable cellular and molecular relationship of target cells' subpopulations alongside therapy. Comparing pre-treatment t2A (Fig. 5A) and post-therapeutic MRD t7A (Fig. 5C) detected by the same iFISH approach, reversed cell quantity ratios of both CTC vs CTEC and small cell vs large cell were observed. When MRD developed, pre-treatment Vim<sup>+</sup> CTCs (Fig. 5A/C) and previously existing PD-L1<sup>+</sup> near-diploid CTCs were no longer detected (Fig. 5B/C). Meanwhile, all detectable MRD CTECs became large multiploid cells and expressed the most aggressive melanoma biomarker Ki67 [27]. Aside from objectively depicting how distinct subtypes of cells are relevant to each other in the metastasis process in Fig. 5, diverse cohorts of patients carrying traceable disparate subtypes of CTCs and CTECs correlating with different clinical outcomes were graphically depicted by Sanky diagram in our previous studies [36,37]. Future combined molecular, cellular and cohort graphic interpretations, along with precision single cell analyses [48,63] of selected diverse subtype of single target cells possessing distinct clinical significance [23,34,36,37,42], will help extensively understand and illustrate how metastatically relevant subcategorized TCs, TECs, CTCs and CTECs either longitudinally proliferate or intra-shift alongside tumor progression.

There is an imperative clinical demand to explore reliable biomarkers that enable predicting and timely evaluating patients' response to therapeutic regimens. The integrated karyotypic and phenotypic tumor tissue and liquid molecular biopsies reported for the first time in

this study, as an in-depth auxiliary approach to the current conventional histopathology biopsy, is more informative for characterization of primary and metastatic tumor lesions, quantitatively delineating the field cancerization and precisely diagnosing metastasis. Not limited to melanoma, unique benefits of biphasic molecular biopsies of subcategorized target cells have also recently been validated and confirmed on different types of carcinomas, such as lung cancer, breast cancer, pancreatic cancer, HCC, cholangiocarcinoma, ovarian cancer, glioma and osteosarcoma, etc. In addition to aneuploidy and tumor marker expression, non-coding RNAs (ncRNAs) in melanoma cells, including microRNAs, long ncRNAs and circular RNAs were all found to participate in regulation of melanoma tumor microenvironment, melanoma cell proliferation, cell cycle, apoptosis, migration, metastasis and therapeutic drug resistance [64].

Further investigation on large cohorts of patients regarding how to objectively define a reliable safety excision margin, how the CD-based risk thresholds of primary lesions and the excision margin assist in risk assessment and stratification for post-operative recurrence, how aneuploid TCs, TECs, CTCs and CTECs undergo phenotypic, karyotypic, morphological and ncRNAs' mutual transition will shed light on a greater in-depth understanding of how those diverse subcategorized cells manifest a functional interplay in therapeutically stressed lymphatic and hematogenous metastatic cascades as well as cancer relapse, thus advancing precision management and ultimately improving cancer patients' outcomes.

#### CRediT authorship contribution statement

**Zhengzheng Fu:** Writing – original draft, Investigation, Formal analysis. **Lina Zhang:** Validation, Formal analysis. **Rongyi Chen:** Investigation, Funding acquisition. **Jipang Zhan:** Investigation. **Jing Zhong:** Investigation. **Wen Zheng:** Investigation. **Jingwen Zou:** Investigation. **Peng Wang:** Investigation. **Xiaohua Deng:** Methodology, Formal analysis. **Alexander Y. Lin:** Writing – original draft, Methodology, Investigation. **Daisy Dandan Wang:** Methodology, Investigation. **Peter Ping Lin:** Writing – review & editing, Investigation, Conceptualization. **Renliang He:** Writing – review & editing, Validation, Supervision, Investigation, Formal analysis, Conceptualization.

#### Declaration of competing interest

The authors declare that they have no known competing financial interests or personal relationships that could have appeared to influence the work reported in this paper.

#### Acknowledgements

Authors thank Drs. Xurong Liu, Qian Zhang, Lai Zhang and staffs at SMU Dermatology Hospital (Guangzhou, China), Cytointelligen (China Medical City, Taizhou, Jiangsu, China) and Cytelligen (San Diego, CA, USA) for providing support. This work was supported by the grant from

Natural Science Foundation of Guangdong Province of China 2016A030313682 and 2020A1515010281 to RC.

## References

- [1] L.E. Davis, S.C. Shalin, A.J. Tackett, Current state of melanoma diagnosis and treatment, *Cancer Biol. Ther.* 20 (11) (2019) 1366–1379.
- [2] B. Domingues, J.M. Lopes, P. Soares, H. Populo, Melanoma treatment in review, *ImmunoTargets Ther.* 7 (2018) 35–49.
- [3] D. Schadendorf, D.E. Fisher, C. Garbe, J.E. Gershenwald, J.J. Grob, A. Halpern, et al., Melanoma, *Nat. Rev. Dis. Prim.* 1 (2015) 15003.
- [4] M. Xu, S. Li, Nano-drug delivery system targeting tumor microenvironment: a prospective strategy for melanoma treatment, *Cancer Lett.* 574 (2023) 216397.
- [5] J. Zhang, A.M. Joshua, Y. Li, C.H. O'Meara, M.J. Morris, L.M. Khachigian, Targeted therapy, immunotherapy and small molecules and peptidomimetics as emerging immunoregulatory agents for melanoma, *Cancer Lett.* 586 (2024) 216633.
- [6] J. Zhao, N. Gao, J. Xu, X. Zhu, G. Ling, P. Zhang, Novel strategies in melanoma treatment using silver nanoparticles, *Cancer Lett.* 561 (2023) 216148.
- [7] A.F. Delgado, A.F. Delgado, Complete lymph node dissection in melanoma: a systematic review and meta-analysis, *Anticancer Res.* 37 (12) (2017) 6825–6829.
- [8] G. Richtig, E. Richtig, A.N. Neiss, F. Quehenberger, D.G. Gmainer, L.P. Kamolz, et al., Does the time interval between sentinel lymph node biopsy and completion lymph node dissection affect outcome in malignant melanoma? A retrospective cohort study, *Int. J. Surg.* 75 (2020) 160–164.
- [9] M.C. van Zeijl, A.J. van den Eertwegh, J.B. Haanen, M.W. Wouters, (Neo)adjuvant systemic therapy for melanoma, *Eur. J. Surg. Oncol. : the journal of the European Society of Surgical Oncology and the British Association of Surgical Oncology* 43 (3) (2017) 534–543.
- [10] C.M. Cornejo, A. Jambusaria-Pahlajani, T.J. Willenbrink, C.D. Schmults, S. T. Arron, E.S. Ruiz, Field cancerization: treatment, *J. Am. Acad. Dermatol.* 83 (3) (2020) 719–730.
- [11] K. Curtius, N.A. Wright, T.A. Graham, An evolutionary perspective on field cancerization, *Nat. Rev. Cancer* 18 (1) (2018) 19–32.
- [12] H. Kadara, I.I. Wistuba, Field cancerization in non-small cell lung cancer: implications in disease pathogenesis, *Proc. Am. Thorac. Soc.* 9 (2) (2012) 38–42.
- [13] A.I. Daud, J.D. Wolchok, C. Robert, W.J. Hwu, J.S. Weber, A. Ribas, et al., Programmed death-ligand 1 expression and response to the anti-programmed death 1 antibody pembrolizumab in melanoma, *J. Clin. Oncol.* 34 (34) (2016) 4102–4109.
- [14] J. Larkin, V. Chiarion-Sileni, R. Gonzalez, J.J. Grob, C.L. Cowey, C.D. Lao, et al., Combined nivolumab and ipilimumab or monotherapy in untreated melanoma, *N. Engl. J. Med.* 373 (1) (2015) 23–34.
- [15] M.W. Lucas, J.M. Versluis, E.A. Rozeman, C.U. Blank, Personalizing neoadjuvant immune-checkpoint inhibition in patients with melanoma, *Nat. Rev. Clin. Oncol.* 20 (6) (2023) 408–422.
- [16] F.F. Gellrich, M. Schmitz, S. Beissert, F. Meier, Anti-PD-1 and novel combinations in the treatment of melanoma: an update, *J. Clin. Med.* 9 (1) (2020).
- [17] S. Cerdido, M. Abrisqueta, J. Sanchez-Beltran, A. Lambertos, M. Castejon-Grinan, C. Munoz, et al., MGRN1 depletion promotes intercellular adhesion in melanoma by upregulation of E-cadherin and inhibition of CDC42, *Cancer Lett.* 581 (2024) 216484.
- [18] D.J. Gordon, B. Resio, D. Pellman, Causes and consequences of aneuploidy in cancer, *Nat. Rev. Genet.* 13 (3) (2012) 189–203.
- [19] G.J. Kops, B.A. Weaver, D.W. Cleveland, On the road to cancer: aneuploidy and the mitotic checkpoint, *Nat. Rev. Cancer* 5 (10) (2005) 773–785.
- [20] L. Garribba, S. Santaguida, The dynamic instability of the aneuploid genome, *Front. Cell Dev. Biol.* 10 (2022) 838928.
- [21] T.A. Potapova, J. Zhu, R. Li, Aneuploidy and chromosomal instability: a vicious cycle driving cellular evolution and cancer genome chaos, *Cancer Metastasis Rev.* 32 (3–4) (2013) 377–389.
- [22] U. Kronenwett, S. Huwendiek, C. Ostring, N. Portwood, U.J. Roblick, Y. Pawitan, et al., Improved grading of breast adenocarcinomas based on genomic instability, *Cancer Res.* 64 (3) (2004) 904–909.
- [23] Y. Li, X. Zhang, D. Liu, J. Gong, D.D. Wang, S. Li, et al., Evolutionary expression of HER2 conferred by chromosome aneuploidy on circulating gastric cancer cells contributes to developing targeted and chemotherapeutic resistance, *Clin. Cancer Res.* 24 (21) (2018) 5261–5271.
- [24] E.R. Shteinman, J.S. Wilmott, I.P. da Silva, G.V. Long, R.A. Scolyer, I.A. Vergara, Causes, consequences and clinical significance of aneuploidy across melanoma subtypes, *Front. Oncol.* 12 (2022) 988691.
- [25] I.A. Vergara, C.P. Mintoff, S. Sandhu, L. McIntosh, R.J. Young, S.Q. Wong, et al., Evolution of late-stage metastatic melanoma is dominated by aneuploidy and whole genome doubling, *Nat. Commun.* 12 (1) (2021) 1434.
- [26] J. Jiang, D.D. Wang, M. Yang, D. Chen, L. Pang, S. Guo, et al., Comprehensive characterization of chemotherapeutic efficacy on metastases in the established gastric neuroendocrine cancer patient derived xenograft model, *Oncotarget* 6 (17) (2015) 15639–15651.
- [27] O. Straume, L. Sviland, L.A. Akslen, Loss of nuclear p16 protein expression correlates with increased tumor cell proliferation (Ki-67) and poor prognosis in patients with vertical growth phase melanoma, *Clin. Cancer Res.* 6 (5) (2000) 1845–1853.
- [28] X. Hong, R.J. Sullivan, M. Kalinich, T.T. Kwan, A. Giobbie-Hurder, S. Pan, et al., Molecular signatures of circulating melanoma cells for monitoring early response to immune checkpoint therapy, *Proc. Natl. Acad. Sci. U.S.A.* 115 (10) (2018) 2467–2472.
- [29] K. Hida, M. Klagsbrun, A new perspective on tumor endothelial cells: unexpected chromosome and centrosome abnormalities, *Cancer Res.* 65 (7) (2005) 2507–2510.
- [30] P.P. Lin, Aneuploid circulating tumor-derived endothelial cell (CTEC): a novel versatile player in tumor neovascularization and cancer metastasis, *Cells* 9 (6) (2020) 1539.
- [31] Q. Zeng, M. Mousa, A.S. Nadukkandy, L. Franssens, H. Alnaqbi, F.Y. Alshamsi, et al., Understanding tumour endothelial cell heterogeneity and function from single-cell omics, *Nat. Rev. Cancer* 23 (8) (2023) 544–564.
- [32] P.P. Lin, O. Gires, D.D. Wang, L. Li, H. Wang, Comprehensive in situ co-detection of aneuploid circulating endothelial and tumor cells, *Sci. Rep.* 7 (1) (2017) 9789.
- [33] H. Dianat-Moghadam, M. Sharifi, R. Salehi, M. Keshavarz, M. Shahgolzari, Z. Amoozgar, Engaging stemness improves cancer immunotherapy, *Cancer Lett.* 554 (2023) 216007.
- [34] Y. Wang, L. Zhang, J. Tan, Z. Zhang, Y. Liu, X. Hu, et al., Longitudinal detection of subcategorized CD44v6(+) CTCs and circulating tumor endothelial cells (CTECs) enables novel clinical stratification and improves prognostic prediction of small cell lung cancer: a prospective, multi-center study, *Cancer Lett.* 571 (2023) 216337.
- [35] Y. Zhao, J. Li, D. Li, Z. Wang, J. Zhao, X. Wu, et al., Tumor biology and multidisciplinary strategies of oligometastasis in gastrointestinal cancers, *Semin. Cancer Biol.* 60 (2020) 334–343.
- [36] L. Zhang, X. Zhang, Y. Liu, T. Zhang, Z. Wang, M. Gu, et al., PD-L1(+) aneuploid circulating tumor endothelial cells (CTECs) exhibit resistance to the checkpoint blockade immunotherapy in advanced NSCLC patients, *Cancer Lett.* 469 (2020) 355–366.
- [37] T. Zhang, L. Zhang, Y. Gao, Y. Wang, Y. Liu, H. Zhang, et al., Role of aneuploid circulating tumor cells and CD31(+) circulating tumor endothelial cells in predicting and monitoring anti-angiogenic therapy efficacy in advanced NSCLC, *Mol. Oncol.* 15 (11) (2021) 2891–2909.
- [38] I. Cima, S.L. Kong, D. Sengupta, I.B. Tan, W.M. Phyto, D. Lee, et al., Tumor-derived circulating endothelial cell clusters in colorectal cancer, *Sci. Transl. Med.* 8 (345) (2016) 345ra89.
- [39] G. Ma, Y. Jiang, M. Liang, J. Li, X. Mao, J.S. Veeramootoo, et al., Dynamic monitoring of CD45-/CD31+/DAPI+ circulating endothelial cells aneuploid for chromosome 8 during neoadjuvant chemotherapy in locally advanced breast cancer, *Therapeutic advances in medical oncology* 12 (2020) 1758835920918470.
- [40] D. Liu, R.W. Jenkins, R.J. Sullivan, Mechanisms of resistance to immune checkpoint blockade, *Am. J. Clin. Dermatol.* 20 (1) (2019) 41–54.
- [41] M.J. Mooradian, R.J. Sullivan, Immunotherapy in melanoma: recent advancements and future directions, *Cancers* 15 (16) (2023).
- [42] X. Liu, J. Li, B.L. Cadilha, A. Markota, C. Voigt, Z. Huang, et al., Epithelial-type systemic breast carcinoma cells with a restricted mesenchymal transition are a major source of metastasis, *Sci. Adv.* 5 (6) (2019) eaav4275.
- [43] P.P. Lin, Aneuploid CTC and CEC, *Diagnostics* 8 (2) (2018) 26.
- [44] A.Y. Lin, D.D. Wang, L. Li, P.P. Lin, Identification and comprehensive Co-detection of necrotic and viable aneuploid cancer cells in peripheral blood, *Cancers* 13 (20) (2021).
- [45] G. Marsavela, C.A. Aya-Bonilla, M.E. Warkiani, E.S. Gray, M. Ziman, Melanoma circulating tumor cells: benefits and challenges required for clinical application, *Cancer Lett.* 424 (2018) 1–8.
- [46] Y.L. Li, X.T. Zhang, S. Ge, J. Gao, J.F. Gong, M. Lu, et al., Clinical significance of phenotyping and karyotyping of circulating tumor cells in patients with advanced gastric cancer, *Oncotarget* 5 (16) (2014) 6594–6602.
- [47] A. Li, Y. Ma, M. Jin, S. Mason, R.L. Mort, K. Blyth, et al., Activated mutant NRas (Q61K) drives aberrant melanocyte signaling, survival and invasiveness via a Rac1-dependent mechanism, *J. Invest. Dermatol.* 132 (11) (2012) 2610–2621.
- [48] Y. Chen, Y. Li, C. Qi, C. Zhang, D. Liu, Y. Deng, et al., Dysregulated KRAS gene-signaling axis and abnormal chromatin remodeling drive therapeutic resistance in heterogeneous-sized circulating tumor cells in gastric cancer patients, *Cancer Lett.* 517 (2021) 78–87.
- [49] A.S. Pierik, C.R. Leemans, R.H. Brakenhoff, Resection margins in head and neck cancer surgery: an update of residual disease and field cancerization, *Cancers* 13 (11) (2021).
- [50] M. Li, F. Gao, X. Ren, G. Dong, H. Chen, A.Y. Lin, et al., Nonhematogenic circulating aneuploid cells confer inferior prognosis and therapeutic resistance in gliomas, *Cancer Sci.* 113 (10) (2022) 3535–3546.
- [51] Y. Hong, J. Si, J. Zhang, Y. Xiong, J. Zhang, P.P. Lin, et al., Small cell size circulating aneuploid cells as a biomarker of prognosis in resectable non-small cell lung cancer, *Front. Oncol.* 11 (2021) 590952.
- [52] C. Xing, Y. Li, S. Wang, H. Zhang, P. Li, M. Dai, CD44+ circulating tumor endothelial cells indicate poor prognosis in pancreatic ductal adenocarcinoma after radical surgery: a pilot study, *Cancer Manag. Res.* 13 (2021) 4417–4431.
- [53] L. Wang, Y. Li, J. Xu, A. Zhang, X. Wang, R. Tang, et al., Quantified postsurgical small cell size CTCs and EpCAM(+) circulating tumor stem cells with cytogenetic abnormalities in hepatocellular carcinoma patients determine cancer relapse, *Cancer Lett.* 412 (2018) 99–107.
- [54] M. Xu, S. Li, The opportunities and challenges of using PD-1/PD-L1 inhibitors for leukemia treatment, *Cancer Lett.* 593 (2024) 216969.
- [55] L. Sinoquet, W. Jacot, L. Gauthier, S. Poudroux, M. Viala, L. Cayrefourcq, et al., Programmed cell death ligand 1-expressing circulating tumor cells: a new prognostic biomarker in non-small cell lung cancer, *Clin. Chem.* 67 (11) (2021) 1503–1512.
- [56] H.A. Parsons, E.R. Macrae, H. Guo, T. Li, W.T. Barry, N. Tayob, et al., Phase II single-arm study to assess trastuzumab and vinorelbine in advanced breast cancer patients with HER2-negative tumors and HER2-positive circulating tumor cells, *JCO Precis Oncol* 5 (2021) 896–903.

- [57] M.A. Khattak, A. Reid, J. Freeman, M. Pereira, A. McEvoy, J. Lo, et al., PD-L1 expression on circulating tumor cells may be predictive of response to pembrolizumab in advanced melanoma: results from a pilot study, *Oncol.* 25 (3) (2020) e520–e527.
- [58] Y. Ouyang, W. Liu, N. Zhang, X. Yang, J. Li, S. Long, Prognostic significance of programmed cell death-ligand 1 expression on circulating tumor cells in various cancers: a systematic review and meta-analysis, *Cancer Med.* 10 (20) (2021) 7021–7039.
- [59] R. Mehrotra, A. Gupta, M. Singh, R. Ibrahim, Application of cytology and molecular biology in diagnosing premalignant or malignant oral lesions, *Mol. Cancer* 5 (2006) 11.
- [60] L.E.B. de Souza, F.U. Ferreira, C.H. Thome, H. Brand, M.D. Orellana, V.M. Faca, et al., Human and mouse melanoma cells recapitulate an EMT-like program in response to mesenchymal stromal cells secretome, *Cancer Lett.* 501 (2021) 114–123.
- [61] K.M. Laurin, K. Coutu-Beaudry, A. Salazar, N. Meribout, E. Audet-Walsh, S. P. Gravel, Low expression of PGC-1beta and other mitochondrial biogenesis modulators in melanoma is associated with growth arrest and the induction of an immunosuppressive gene expression program dependent on MEK and IRF-1, *Cancer Lett.* 541 (2022) 215738.
- [62] S. Li, S. Luo, N. Wei, A.Y. Lin, D.D. Wang, P.P. Lin, et al., A rare case of Merkel cell carcinoma on the craniofacial region and characterization of its aneuploid CD31(-) CTCs and CD31(+) CTECs expressing EpCAM or Ki-67, *Oral Oncol.* 147 (2023) 106602.
- [63] X. Hu, Z. Hu, H. Zhang, N. Zhang, H. Feng, X. Jia, et al., Deciphering the tumor-suppressive role of PSMB9 in melanoma through multi-omics and single-cell transcriptome analyses, *Cancer Lett.* 581 (2024) 216466.
- [64] F. Liu, S. Li, Non-coding RNAs in skin cancers: Biological roles and molecular mechanisms, *Front. Pharmacol.* 13 (2022) 934396.